ARTICLE IN PRESS

Communications Medicine

https://doi.org/10.1038/s43856-026-01551-4

Article in Press

Mitochondrial hyperoxidation contributes to warm ischemia-reperfusion injury in rat and pig livers

Received: 23 October 2024

Accepted: 5 March 2026

Cite this article as: Nguyen, K.T., Ozgur, O.S., Jain, R. *et al.* Mitochondrial hyperoxidation contributes to warm ischemia-reperfusion injury in rat and pig livers. *Commun Med* (2026). https://doi.org/10.1038/s43856-026-01551-4

Khanh T. Nguyen, O. Sila Ozgur, Rohil Jain, Christopher Taveras, Emmanuella O. Ajenu, Tyler Pugeda, Alona Muzikansky, Seyed Alireza Rabi, Asishana A. Osho, John N. Kheir, Daryoosh Vakhshoori, Korkut Uygun, Padraic Romfh & Shannon N. Tessier

We are providing an unedited version of this manuscript to give early access to its findings. Before final publication, the manuscript will undergo further editing. Please note there may be errors present which affect the content, and all legal disclaimers apply.

If this paper is publishing under a Transparent Peer Review model then Peer Review reports will publish with the final article.

ARTICLE IN PRESS

© The Author(s) 2026. **Open Access** This article is licensed under a Creative Commons Attribution-NonCommercial-NoDerivatives 4.0 International License, which permits any non-commercial use, sharing, distribution and reproduction in any medium or format, as long as you give appropriate credit to the original author(s) and the source, provide a link to the Creative Commons licence, and indicate if you modified the licensed material. You do not have permission under this licence to share adapted material derived from this article or parts of it. The images or other third party material in this article are included in the article's Creative Commons licence, unless indicated otherwise in a credit line to the material. If material is not included in the article's Creative Commons licence and your intended use is not permitted by statutory regulation or exceeds the permitted use, you will need to obtain permission directly from the copyright holder. To view a copy of this licence, visit http://creativecommons.org/licenses/by-nc-nd/4.0/.

ARTICLE IN PRESS

Mitochondrial hyperoxidation contributes to warm ischemia-reperfusion injury in rat and pig livers

Khanh T. Nguyen[1,2,*], O. Sila Ozgur[1,2,*], Rohil Jain[1,2], Christopher Taveras[1,2], Emmanuella O. Ajenu[1,2], Tyler Pugeda[1,2], Alona Muzikansky[3], Seyed Alireza Rabi[4], Asishana A. Osho[4], John N. Kheir[5], Daryoosh Vakhshoori[6], Korkut Uygun[1,2], Padraic Romfh[6], Shannon N. Tessier[1,2,#].

[1] Center of Engineering in Medicine and Surgery, Department of Surgery, Massachusetts General Hospital – Harvard Medical School, Boston, Massachusetts, United States of America
[2] Shriners Hospital for Children – Boston, Boston, Massachusetts, United States of America
[3] Biostatistics Center, Massachusetts General Hospital – Harvard Medical School, Boston, Massachusetts, United States of America
[4] Division of Cardiac Surgery, Department of Surgery, Massachusetts General Hospital – Harvard Medical School, Boston, Massachusetts, United States of America
[5] Department of Cardiology, Boston Children's Hospital – Harvard Medical School, Boston, MA
[6] Pendar Technologies, Cambridge, Massachusetts, United States of America

[*] These authors contributed equally to this work.
[#] The corresponding author. Email: sntessier@mgh.harvard.edu

ARTICLE IN PRESS

ARTICLE IN PRESS

Abstract

Background: Mitochondrial dysfunction is a critical factor in several diseases, but current *in situ* assessment methods are severely limited. Non-invasive monitoring of mitochondrial redox state using resonance Raman Spectroscopy (RRS) offers a promising solution. This study aims to demonstrate RRS utility with liver models of warm ischemia-reperfusion injury in organ transplantation. **Methods**: Lewis rat (female) and Yorkshire pig (both sexes) livers were evaluated during reperfusion by subnormothermic machine perfusion, with 3-6 replicates per study group, and statistical comparisons using unpaired two-tailed Student's t-tests with Welch's correction for potentially unequal variance. RRS provides *in situ* quantification of the overall mitochondrial redox state, and herein further refined to resolve the redox state of individual complex III and IV. **Results:** Here we show that RRS can differentiate non-viable rat livers (3h warm ischemia, WI) from viable 1h WI and fresh controls as early as 30 mins into reperfusion. RRS also identifies dysfunction at complex III characterized by hyperoxidation during reperfusion. This guides us to test methylene blue, which acts as an alternate electron donor to bypass complex III, as treatment rescuing mitochondria from WI-induced reperfusion injury. When tested on pig marginal livers with extended WI (30-45 mins), our RRS-guided treatment enables recovery of hemodynamics and oxygen/lactate values that approached controls without WI. **Conclusions:** RRS assessment and guided treatment with methylene blue provide two lines of evidence indicating that mitochondrial hyperoxidation, specifically at complex III, is a critical mechanism underlying warm ischemia-reperfusion injury. This study demonstrates the potential of RRS for transplantation and broader applications.

Plain Language Summary

Healthy mitochondria are crucial for organ function, and their functional failure contributes to poor organ transplantation outcomes. In this study, we used a light-based method called resonance Raman spectroscopy (RRS) to assess mitochondrial health directly on the liver surface, without removing tissue. We find that long periods of warm ischemia (i.e., no blood flow at body temperature) caused significant mitochondrial stress, especially at complex III, which is important for energy production. We then tested methylene blue, an FDA-approved drug that helps mitochondria maintain function while bypassing complex III. In pig livers with injury similar to marginal human donor organs, methylene blue improves oxygen use and blood flow profiles. These results highlight the potential of RRS for improving transplant outcomes.

ARTICLE IN PRESS

ARTICLE IN PRESS

Introduction

Mitochondria are highly studied in cell physiology and pathology (reviewed in [1]) because they stand at a critical intersection between life and death, comprising the complex pathways that direct metabolism as well as those key to injury. The central element of mitochondrial function is the electron transport chain (ETC), which consists of four complexes (cI, cII, cIII, cIV) in the inner mitochondrial membrane that use electron flow to create an electrochemical gradient and power ATP generation at complex V (cV). Under physiological conditions, much of the oxygen consumed during oxidative phosphorylation is reduced to water; however, a portion of electrons leak along the ETC and covalently reduce oxygen to form the highly reactive superoxide (ROS) [2, 3]. While some ROS is essential for normal cell signaling, significant changes may lead to metabolic dysfunction, oxidative cell damage, and programmed cell death, which are defining features of countless disease states [4]. Although extensive research has investigated the role of mitochondria in various tissues and disease states [5-8], the precise sequence of events and underlying mechanisms of mitochondrial injury remain poorly understood.

Several techniques are currently employed to assess mitochondrial injury, including both direct and indirect methods, each with distinct advantages and limitations. For instance, indirect assessments may involve measuring coenzymes such as NADH and $FADH_2$, which transfer electrons within the ETC; ATP, the primary energy output of mitochondria; or mitochondrial breakdown products like cell-free flavin mononucleotide (FMN), as others have done in liver transplantation [9, 10]. While these biomarkers offer valuable insight into mitochondrial function and injury, they do so through indirect means. Direct assessments offer more specific evaluations but present additional challenges. For example, mitochondrial membrane potential (MMP), typically measured using cationic dyes, serves as a widely used indicator of mitochondrial dysfunction. However, MMP does not reveal the precise site or mechanism of injury [11, 12]. Other direct analytical techniques, such as electron microscopy and mitochondrial respirometry, can yield detailed structural and functional data but require tissue sampling and specialized processing. While these methods have been applied in liver transplantation contexts [13], the need for tissue samples can pose practical limitations, particularly in clinical or time-sensitive settings [14, 15]. Instead, our team [16-18] have been developing technology to rapidly and dynamically measure the redox states of whole mitochondria from the surface of whole organs without the need for tissue processing. We take advantage of the distinct heme structures present in mitochondrial cytochromes, which generate resonance Raman scattering events that are captured and quantified with our custom-built Resonance Raman Spectroscopy (RRS) device.

To demonstrate the advantage of our RRS device to better understand mitochondrial dysfunction from a dynamic perspective, we interrogated the mitochondrial redox state as a function of ischemia-reperfusion injury (IRI) in the context of liver transplantation. Mitochondrial injury significantly contributes to the IRI development since the organelle's integrity is highly sensitive to oxygen supply changes as seen in ischemia and reperfusion events [19]. Exposure to warm ischemia (WI), whereby the organ remains *in situ* at body temperature without circulatory support, poses a significant risk for organ viability as it leads to decreased patient and graft survival rates [20-22]. In light of this, limits on WI time as well as other criteria (e.g. steatosis, fibrosis, perfusate chemistry, etc.) have adversely impacted the utilization of Donation after Circulatory Death (DCD) liver, which remained low at 20-25% in the USA over the last 10 years [23]. As DCD is increasingly considered for the purpose of alleviating severe shortages of viable organs [24-26], there is a critical need to safely increase the utilization of DCD livers. Leveraging RRS technology, we aim to elucidate mechanisms of WI-induced mitochondrial injury, specifically those that could lead to future development of IRI prevention/recovery strategies aimed at improving/preserving the viability of DCD livers for transplantation.

In this study, we first characterize the overall mitochondrial redox state, which is defined as the ratio of reduced to total mitochondria (or Resonance Raman Reduced Mitochondrial Ratio:

ARTICLE IN PRESS

3RMR), in rat DCD liver models with incremental WI time and a subnormothermic machine perfusion (SNMP) protocol previously established by our team [16, 27]. Herein, we also enhance the capabilities of our RRS approach by developing methods to selectively measure the redox states of individual complexes (cIII and cIV) in the ETC non-invasively from the surface of mammalian livers, thereby facilitating mechanistic insights into mitochondrial injury during ischemia-reperfusion injury that were otherwise not possible. In specific, we optimize our regression library for specific measurement of individual complexes of the ETC, including cIII and cIV, to identify the precise location of injury leading to mitochondrial dysfunction (i.e., 3RMR_CIII and 3RMR_CIV). Through this process, we discover that livers exposed to severe ischemic events exhibit hyperoxidation at cIII during reperfusion. This knowledge provided us with an opportunity to investigate the application of methylene blue (MB), an FDA-approved drug that shuttles electrons from cI to cytochrome c (which are then transferred to cIV), therefore bypassing cIII [28]. When added to the perfusate, MB results in the complete oxidation of cIII and increases the reduced state of cIV, supporting its expected mode of action. Importantly, this rescues rat liver mitochondria from IRI-mediated injury during machine perfusion, both with and without hemoglobin-based oxygen carrier (HBOC) to enhance oxygen delivery. Finally, we showcase the translational potential of our RRS-guided treatment through the MB-supplemented perfusion on DCD pig livers with extended WI time (i.e., 45 mins) that are expected to be non-transplantable, showing recovery of hemodynamics and oxygen/lactate values, with no statistical differences with transplantable DBD (Donation after Brain Death) controls. Additionally, results from MB treatment further validates the RRS finding of mitochondrial hyperoxidation. Since MB specifically targets dysfunction at cIII, its efficacy offers functional evidence that hyperoxidation at cIII is a true driver of the WI-induced reperfusion injury. Overall, our study demonstrates how unique bioengineering advances can be used to enhance mechanistic understanding of mitochondrial dysfunction and how these insights can be leveraged to therapeutically intervene and rescue DCD livers from IRI. Ultimately, these insights and strategies could be used to make more DCD livers available for transplantation as well as better understand IRI across broad pathological conditions.

ARTICLE IN PRESS

ARTICLE IN PRESS

Methods

Ethical statement

All the experimental protocols were approved by Institutional Animal Care and Use Committee (IACUC) of Massachusetts General Hospital (Boston, MA, USA; 2023N000107, 2023N000042), All experiments were performed in accordance with relevant guidelines and regulations, including the ARRIVE guidelines for reporting animal experiments.

Experimental Design

Rat: For the initial step, the effect of different durations of warm ischemia (WI) on the liver viability was investigated. 18 rat livers were divided into 3 experimental groups (n=6 per group): 1-hour warm ischemia (1h WI), 3 hours warm ischemia (3h WI), and fresh livers (no WI) as control. The livers underwent subnormothermic machine perfusion (SNMP) at room temperature (21°C) for 3 hours with an acellular solution. Supplementarily, 12 rat livers (n=3 per group: fresh, 1h WI, 3h WI, and Fresh+Antimycin A) were used separately to perform oxygen stress tests. For these livers, SNMP was performed for 90 mins with acellular solution and then livers were subjected to a complete pause of both perfusate fluid flow and oxygen air supply for a dynamic RRS evaluation of mitochondrial response to acute ischemic stress.

Next, the effects of MB and HBOC were investigated in the 3h WI group. For this step, a total number of 6 livers were divided into 2 experimental groups (n=3 per group): 3hWI treated with MB (3hWI+MB) and 3hWI treated with both MB and HBOC (3hWI+MB+HBOC). The livers were subjected to SNMP for 3 hours using acellular solution combined with the treatments. Here, the 3h WI (no treatment) group served as the control for evaluating therapeutic effects.

Pig: Finally, the effects of MB and HBOC were investigated using 17 DCD pig livers, which were allocated into four groups for study. The first group (30minWI, n=4) underwent 3-hour SNMP without treatment after a 30-minute WI period. The second group (30minWI+MB+HBOC, n=5) received a combined treatment of MB and HBOC during SNMP following the same WI period. The third group (45minWI+MB, n=4) was subjected to an extended 45-minute WI period, followed by treatment with MB alone during 3-hour SNMP, to assess the effects of MB on liver with extended WI during SNMP. The fourth group (Fresh DBD, n=4) was procured without any WI time and immediately put on an SNMP system. Here, the 30minWI (no treatment) group served as the primary control for assessing therapeutic benefits, as improvements compared to this group directly indicate treatment effectiveness. The fresh DBD group served as a complementary benchmark to contextualize how closely the treated livers approach functional performance under ideal conditions. Given the anatomical and physiological similarities between pig and human livers, we expect findings in our pig liver models to have relevance for human biology and could support subsequent translational research.

Animal Housing and Liver Procurement

Rat: The experimental protocols were approved by the IACUC of Massachusetts General Hospital (Boston, MA, USA; 2023N000107). Livers from healthy, adult female Lewis rats (strain code 004, 10-12 weeks old, weighing 175-200 g) (obtained from Charles River Laboratories, Wilmington, MA, USA) were used for all experiments to ensure the consistency between groups. All animals were received pathogen-free and non–genetically modified (wild-type), with no procedures or treatments before experiments. They were housed socially in a temperature and humidity-controlled room and provided unrestricted food and water. The liver was procured as previously described [29]. Briefly, rats were heparinized and bile ducts were cannulated. The splenic and gastric branches of the portal vein, as well as the hepatic artery, were ligated. The portal vein was cannulated with a 16-gauge catheter and flushed with 40 mL of heparinized saline (1000 U/mL,

room temperature). After freeing the liver, an additional 20 ml of heparinized saline was flushed to clear any remaining blood from the organ. Rats were completely anesthetized with isoflurane during surgical procedures to minimize pain and distress. They were also monitored throughout the procedures, and no unexpected adverse events were observed. During the final flush, rats were euthanized as results of the exsanguination. Humane endpoints were not required because all procedures occurred under anesthesia and animals were euthanized at the planned endpoint. Perfusion was started immediately after procurement for fresh group. For WI groups, following procurement, the liver was placed in a temperature-controlled chamber with saline and maintained at 36 ± 0.1°C for either 1 hour or 3 hours.

Pig: The experimental protocols were approved by the IACUC of Massachusetts General Hospital (Boston, MA, USA; 2023N000042). Healthy male and female Yorkshire pigs (3-4 months old, around 40 kg) were obtained from CBSET (Lexington, MA, USA) one week before surgery to allow acclimatization. All animals were received pathogen-free and non–genetically modified (wild-type), with no procedures or treatments before experiments. They were housed in a temperature and humidity-controlled room and provided unrestricted food and water. The liver was procured as previously described [30, 31]. Briefly, the pigs were sedated with atropine (0.04mg/kg), telazol (4.4 mg/kg), and xylazine (2.2 mg/kg), and A bolus of Propofol (0.16-0.33 mg/kg) was administered through the IV line. General anesthesia was maintained via continuous isoflurane (3-5%) inhalation and intravenous fentanyl (5-20 ug/kg/h) as needed to minimize pain and distress. Heart rate, blood pressure, oxygen saturation and ventilation were monitored, and no unexpected adverse events were observed. After a bolus of heparin (100 U/kg) was administered, a midsternal incision and sternotomy, the descending aorta was cannulated [32], and laparotomy was performed. Next, for donation after circulatory death (DCD) livers, the animal was switched to intravenous anesthesia, and the ventilator was turned off, allowing the animal to undergo cardiac arrest. Once the mean arterial pressure (MAP) fell below 30 mmHg, a 30-minute timer started to track the warm ischemic time. For extended WI, liver was left unflushed for an extra 15 minutes (45 minutes total) in the abdominal cavity. For donation after brain death (DBD) livers, hemodynamic support was maintained to ensure stable circulation with the MAP was kept at ≥60 mmHg (no WI) throughout the procurement. For all livers, immediately after cross-clamp and flush initiation through the aorta, the portal vein was cannulated and secured with 2.0 Prolene suture. Once livers were flushed with 1L of cold (4 °C) Lactated Ringer's solution followed by 1L of University of Wisconsin (UW) cold storage solution, the surrounding structures were carefully cut with a wide incision around the hilum, and the liver was removed from abdominal cavity. Livers were prepared on the back table by cannulating the portal vein, hepatic artery, and bile duct, and by removing the gallbladder. This was followed by flushing out the UW solution with 2L of cold (4 °C) Lactated Ringer solution through portal vein (1.5 L) and hepatic artery (0.5 L) shortly before initiating the perfusion. The liver was connected to the perfusion machine after the vessels were prepared on the back table while livers were kept on ice. Humane endpoints were not required because all procedures occurred under anesthesia and animals were euthanized at the planned endpoint.

Machine Perfusion

Setup and Operations

Rat: The perfusion system setup and operation are previously described [33]. Briefly, the flow rates were manually adjusted for the maximum pressure of 5 mmHg and temperatures were maintained at subnormothermic temperatures (SNMP, ~21°C). The system was first primed with perfusate to confirm that the recirculation loop was leak-free, tubing was bubble-free, and flow of gas (95% O_2 and 5% CO_2) was adequately delivered to oxygenator. Then, the liver was connected to the system by an 18-gauge catheter and experiment began. Liver weight was measured before

and after SNMP time to calculate weight gain (%) during SNMP. RRS measurements and perfusate sampling were performed within the first 10 mins, then at 30, 60, 90, 120, 150 and 180 mins of SNMP for liver viability assessment. For 1h WI and 3h WI livers, an additional RRS measurement was performed after WI, just before connecting livers to the perfusion system and was reported as T=0 mins of SNMP time; this T=0 time-point was not available for fresh livers since they were immediately connected to the system after procurement without WI. At the end of SNMP, tissue samples were collected for liver energy status and histology evaluations. The oxygen stress test (OST) involved transitioning from continuous oxygenated perfusion (i.e., SNMP) to acute ischemia by stopping both perfusate flow and oxygen delivery. RRS measurements were performed throughout this transition time.

Pig: SNMP was initiated using a device that enables dual perfusion through the portal vein and hepatic artery in a closed circuit (Liver Assist Organ Assist, Groningen, Netherlands), as previously described [30, 31]. Briefly, the pressures were set to 5 mmHg for the portal vein and 55 mmHg for the hepatic artery, the flow rates were automatically adjusted, and the temperature of the system was set to 21°C. RRS measurements were performed shortly before the start of perfusion (T=0 min), within the first 10 mins of SNMP (T=10 mins), and then at 30, 60, 90, 120, 150 and 180 mins of SNMP. Perfusate samples were collected within the first 10 mins, then at 30, 60, 90, 120, 150 and 180 mins for other liver viability assessments. Flash-frozen tissue samples were collected at the beginning and at the end of SNMP for evaluation of energy status. Wedge biopsies were collected at the end of SNMP for histology.

Perfusate Preparation

Rat: The perfusion solution consisted of 500 mL phenol red-free Williams' Medium E (Sigma-Aldrich, St Louis, MO, USA) supplemented with 5 g bovine serum albumin (Sigma-Aldrich, USA), 12 mg water-soluble dexamethasone (Sigma-Aldrich, USA), 5 mL penicillin-streptomycin (Thermo Fisher Scientific, Waltham MA, USA), 5 ml L-glutamine (Sigma-Aldrich, China), 2.5 uL insulin (MGH Pharmacy), 1000 U heparin (MGH Pharmacy), as previously described [30, 31]. For the experimental groups containing antimycin A (AA), these livers received a direct bolus injection of AA (10 mL of 1 mM) during SNMP. This dose was then recirculated within SNMP system containing 500 mL of perfusate, yielding a final AA concentration of ~0.02 mM. For the experimental groups containing methylene blue (provided by Beantown Chemical, Hudson, NH, USA), a total dose of 50 mg of MB drug for 500 mL of perfusate was administered in the following fashion: initial 25 mg MB (0.05 mg/mL) shortly prior to SNMP to allow uniform distribution of MB within the perfusion system, followed by an additional 5 mg MB (0.001 mg/mL) at T= 30, 60, 90, 120, and 150 minutes. MB doses were adapted from previous study in rat models [34]. For 3hWI+MB+HBOC group 25% HBOC-201 v/v (provided by Hemoglobin Oxygen Therapeutics, Souderton, PA) was added to the solution.

Pig: The same acellular Williams' E based solution was used with a volume of 2L for each pig liver perfusion. The 30minWI group was perfused only with acellular solution. The 30minWI+MB+HBOC group was supplemented with MB and HBOC as described above.

Mitochondrial Redox State Assessment by RRS device

Device Components and Measurement Overview

The RRS system by Pendar Technologies consists of several key components: a 441 nm laser pump source, a fiber optic probe with coaxial light emission and collection, and a high-resolution spectrometer. The laser delivers 8mW of single-line excitation light, which is focused into a 1.5 mm spot located 9 mm from the probe tip. The scattered light from the sample is collected, passed through a filter to remove the excitation signal, and then directed to the spectrometer. The spectrometer has a resolution of 8 cm^{-1} (FWHM) and includes an internal acetaminophen

ARTICLE IN PRESS

calibration reference to ensure accuracy. The system uses a temperature-controlled image sensor to maintain consistent dark current and cosmic rays are eliminated from the Charge-Coupled Device (CCD) signal before processing. Spectra are captured every second and integrated over a 180-second period for analysis.

The RRS measurements were taken on the liver surface at the center of the left lobe, as recommended by our previous study [16], which identified this as the optimal site for assessing mitochondrial redox state as an indicator of whole-organ viability. In that study, 3RMR_mito values were compared across three positions: P1 (center of the left lobe), P2 (periphery of the left lobe), and P3 (center of the right lobe). Central regions (P1 and P3), which lie closer to major vessels and are more likely to receive uniform oxygenation during machine perfusion, yielded similar 3RMR_mito values within the same liver and showed a progressive divergence between viable (24 h cold ischemia) and non-viable (72 h cold ischemia) groups over the 3-hour perfusion period. Additionally, measurements at P1 showed a significant difference between these groups at 3 hours and exhibited a strong correlation with oxygen consumption, an established indicator of whole-organ respiratory performance. In contrast, the peripheral region (P2) displayed transiently higher 3RMR_mito values during early reperfusion, which still converged with central measurements between 60 and 180 minutes of perfusion. This pattern is expected because tissue further from major vessels requires additional time to achieve adequate perfusion, leaving it more reduced than central regions during early reperfusion time. The observed spatial heterogeneity is also consistent with other reports of spatial differences in IRI [35, 36]. At P2, group differences decreased over time, which is opposite to the progressive divergence observed at central sites and in other whole-organ viability metrics. Together, these findings established measurements at central regions as a reliable site for evaluating mitochondrial redox state as an indicator of whole-organ viability, a choice further supported in a follow-up study examining reoxygenation dynamics under different perfusates [17].

Because the objective of the pig liver experiments was aligned with that of the rat studies, namely using RRS-derived mitochondrial redox state as an indicator of overall graft viability, the use of a standardized RRS measurement site that could reflect global graft viability is still a reliable approach. Given similarities between rat and pig livers, particularly the presence of larger vessels in central lobar regions and a prominent left lateral lobe in both species, we adopted the central region of the left lobe as the standardized measurement site for pig liver experiments. In addition, we include here a preliminary dataset evaluating RRS measurements at the central regions of different lobes (right, caudate, left) in human livers to provide cross-species validation of our measurement RRS approach for assessing overall graft viability. Study protocol was approved by the Institutional Review Board (IRB) of Massachusetts General Hospital (Boston, MA, USA; 2012P001090); no registration (i.e., clinicaltrial.gov) was required because this was not a clinical trial. Recruitment criteria were standard and included adults aged 18 years or older of both sexes, and from diverse racial backgrounds. Three discarded human livers were acquired from New England Donor Services (NEDS, Waltham, MA, USA) after being declined by all transplant centers because of clinical risk factors and total cold/warm ischemia time, with key donor characteristics reported in **Supp. Table 1**. Organ procurement was performed according to standard clinical practice at the discretion of the surgeons No organs were procured from prisoners. Informed consent was obtained from all participants. Livers were transported in ice-cold preservation solution (4–6 °C) via static cold storage. Upon arrival at our laboratory, livers were kept at 4-6^{o}C for up to another 6 hours to back-table preparation before experiments. Then, RRS was obtained from biopsies sampled at the central regions on the left, caudate and right lobes in each liver **(Supp. Fig. 1a)** using a 2-mm diameter tissue punch. Liver biopsies were also subjected to oxygenated perfusion for about 15 mins prior to RRS measurement for assessment of liver viability during reperfusion phase. Here, the results suggest that intra-differences due to spatial differences within a single liver are smaller than the inter-differences between different livers **(Supp. Fig. 1b)**. Two-way ANOVA reports that spatial locations (intra-differences) accounted for only 3.6% ($p=0.6305$) of the total variance, whereas variability between livers (inter-

differences) accounted for 82.36% (p=0.0211), which is as expected because discarded human grafts naturally vary widely in quality. These findings indicate that when RRS measurements are taken at regions consistent with our defined criteria, including closer proximity to major blood vessels and possibly more uniform oxygenation, 3RMR_mito values remain consistent across different lobes and reliably reflect overall liver quality. This is consistent with our prior rat liver data (which showed similar 3RMR_mito values between central regions of the left and right lobes) and further validate the use of our standardized measurement site to evaluate overall graft viability in larger livers, such as those from pigs and humans.

Library Creation

Whole mitochondria isolation procedure: Chromophores for the mitochondrial library were developed by Pendar in partnership with the National Institutes of Health Cardiac Energetics Laboratory and based on previous experiments [18, 37]. Fresh whole mitochondria were isolated from rat and rabbit hearts, as described previously [37]. Briefly, hearts were perfused in situ with Krebs-Hanseleit buffer to remove blood and supply calcium before excision. After removing fat and connective tissues, the left ventricles and septa were dissected, weighed, and minced with scissors in an isotonic ice-cold buffer A (0.28M sucrose, 10 mM HEPES, 1 mM EDTA, 1 mM EGTA, and 5 mM K_2HPO_4 and KOH to adjust pH to 7.1). The minced tissue was diluted with buffer A to a 10% w/v suspension and disrupted in a tissue homogenizer over ice. It was then treated with 2.5 mg/5 g tissue wet weight of trypsin at 4°C for 15 min. This was followed by stopping the trypsin activity by adding 13 mg/5 g tissue wet weight of trypsin inhibitor and 100 mg/10 mL of bovine serum albumin. The homogenate was then centrifuged at 600 g for 10 min at 4°C to collect the supernatant containing mitochondria. The pellet was resuspended in buffer A and homogenized before centrifuged again at 600 g for 10 min at 4°C. The supernatant was collected and pooled with the previous supernatant. The pellet was resuspended in 40 mL buffer A and recentrifuged at 600 g for a total of three times, where the subsequent supernatants are combined. The final pooled supernatant containing the mitochondria was then centrifuged at 8000 g for 10 min at 4°C to pellet the isolated mitochondria. The pelleted mitochondria were resuspended in buffer A, followed by another 8000 g centrifugation. The pelleted mitochondria were washed and resuspended in buffer B (125 mM KCl, 15 mM NaCl, 20 mM Hepes, 1 mM EGTA, 5 mM $MgCl_2$, 5 mM potassium phosphate pH 7.1). This was followed by another centrifugation at 8000 g and resuspension in 1 mL buffer B. This mitochondrial suspension is further purified using Percoll gradient centrifugation, as described previously [38], to remove broken mitochondria and cell debris. The final mitochondrial suspension in buffer B was quantified spectroscopically for its Cytochrome a content as a reference, as described previously [39].

Whole mitochondria library generation: The purified mitochondrial samples were then exposed to oxidizing versus reducing conditions. Briefly, a 350 mL sample of 4 nmol cyt a/mL solution in Fiskum Buffer was placed in a 1 mL cuvette and exposed to environmental oxygen to produce the oxidized form. To fully reduce the sample, a small amount of hydrogen sulfide (HS) was added, and nitrogen was blown over the cuvette before the cap was replaced. These preparations were contained in a glass vial and placed 9 mm from the RRS probe while shielding from room light to collect the spectra for a period of 600 seconds. The spectra were averaged, and the baseline fluorescence background was subtracted to produce a pure spectrum for the oxidized/reduced state of the whole mitochondria, which was added to the library. A clear difference in RRS was observed because of exposure to oxidizing versus reducing conditions, which can be visualized as differences in peak positions and intensities in the Raman spectrum, as shown in **Fig. 1b** and **Supp. Fig. 2**.

Complex III & IV isolation procedure: In addition to the spectra for whole mitochondria, we also purified individual complexes III (cIII) and IV (cIV) of the electron transport chain, as previously described [40]. We focus on cIII and cIV since both are rich in heme groups with resonant Soret band absorption in the ~430–450 nm range [41, 42], which overlaps with our 441 nm excitation wavelength. These properties result in their strong and spectrally distinct Raman signals, as shown in **Supp. Fig. 2**. In contrast, Complex I (cI) is not Raman-active under our conditions due

to the absence of a heme group [43, 44]. While complex II (cII) may be Raman active with a Soret peak of 416/426 [45], it is present at relatively lower concentrations, as compared to cIII [46], and hence was not captured in the present study (confirmation of this is provided in **Supp. Fig. 3** and described further under *Complex III & IV library generation* below).

The cIII and cIV are isolated using a procedure described previously [37, 40]. Briefly, a stock sample of isolated mitochondria (corresponding to 200 nmoles of cytochrome a) is used as the starting material. The mitochondria are diluted to 10 nmol cytochrome a/mL in ice-cold buffer C (50 mM Tris, 1mM $MgSO_4$, pH 8.45). Then, 10% w/v n-β-D-dodecyl maltoside (DM) is added dropwise to a final concentration of 1% with gentle mixing on ice. The extract was centrifuged at 40,000 g for 40 min at 4°C, and the supernatant was applied to a 2.5 x 20 cm glass column (Bio Rad), previously packed with DEAE Sepharose Fast Flow anion exchange resin (GE Healthcare) equilibrated with 5 column volumes of buffer C (containing 0.02% w/v DM). After washing with 2 column volumes of buffer C, elution of mitochondrial complexes was achieved by applying a linear 0-400 mM NaCl gradient in the same buffer and collecting the elute in 4 mL fractions. Green fractions containing cIV eluted close to the middle of the gradient (~180mL NaCl), before the reddish fractions containing cIII. The pooled fractions containing each complex were concentrated to 20-30 nmoles cytochrome a/mL.

Complex III & IV library generation: Once the individual complexes were isolated, each complex was then exposed to oxidizing and reducing conditions. An 11 mM sample of cIII in Tris buffer was reduced using 2 mL of ascorbate (1 M) to reduce cytochrome c1 and 2mL of HS to fully reduce cytochromes b_L and b_H. An 18.67 mM sample of cIV in Tris buffer was reduced in multiple steps as cIV undergoes a catalytic oxidation process with multiple states [47]. To fully reduce cIV, two additions of 2 mL of H_2O_2 (10 mM) were made followed by 2 mL of HS to produce the fully reduced form. Library spectra were collected after each addition to capture each step of the cycle. Fully oxidized and reduced spectra were added to the final reference library to represent the steady states of cIV. All samples were prepared in a 1 mL glass vial which was held in a fixed position at 9 mm from the probe lens and enclosed by a black box to prevent light contamination. RRS spectra were collected for 600 seconds for each complex and oxidation state.

To visually illustrate the spectral differences between cIII versus cIV as well as whole mitochondria versus individual complexes, we present **Supp. Fig. 2** and **Supp. Fig. 3,** respectively. **Supp. Fig. 2** shows the spectral differences (in peak positions and intensities) between redox states of the same complex (**a-d**) versus differences between complexes (**e-h**) at 441 nm excitation wavelength. For example, in **Supp. Fig. 2e,** the oxidized state of cIII and cIV are shown as a red solid and red dotted line, respectively, while the corresponding computed differences (generated by subtracting one spectrum from the other) are shown in the panel below as a black line (i.e., **Supp. Fig. 2f**). Here, the ν_4 band, centered around 1370–1380 cm^{-1}, differs between cIII and cIV, with cIII exhibiting sharper, lower-frequency peaks, while cIV shows broader, upshifted bands. While we highlight this one example at the ν_4 band (1370–1380 cm^{-1}), it should be noted that our regression analysis determines the best fit of the experimental spectra against the library of known spectra across the full range (700 to 1500 cm^{-1}).

To show the relationship between spectra from whole mitochondria versus individual complexes, we include **Supp. Fig. 3.** The 441nm excitation source is close to the Soret absorption maximum of reduced cIV, which results in maximal resonant enhancement of this chromophore. A regression using the reduced cIII and cIV libraries (**Supp. Fig. 3a**) fully explains the measured spectrum of reduced mitochondria, resulting in minimal unexplained residual (shown as a black line). Using only the cIII (**Supp. Fig. 3b**) or cIV (**Supp. Fig. 3c**) reduced library does not fully explain the spectrum from whole mitochondria and results in a non-random structure in the residual especially near the ν_4 band around 1356 cm^{-1}. In short, the sum of the individual spectrum of cIII and cIV are differentiated and together fully explain the spectrum of the whole mitochondria.

Generation of other libraries: Libraries were also created for hemoglobin and included in the regression algorithm when HBOC was present during perfusion. Fresh blood was collected via

exsanguination of a rat and oxygenated in a cuvette using 100% oxygen (fully oxygenated) or deoxygenated using sodium dithionate (fully deoxygenated). Resonance Raman spectra were created by imaging through the glass cuvette wall. A small stirring magnet at the base of the cuvette was used to mix the solution. To produce oxygenated state, a pure oxygen headspace was established inside the cuvette. Whereas, to produce deoxygenated state, sodium dithionate was added and a pure nitrogen headspace was established. Spectra in the oxygenated and deoxygenated states were measured for 10 minutes. The resonance Raman spectra show unique markers, especially at the ν_4 band, where the peak at 1356 cm^{-1} is the deoxygenated Hb peak and 1376 cm^{-1} is the oxygenated Hb peak. Finally, additional spectral profiles of methylene blue and the base perfusate were also investigated; however, since there were no Raman-active components (see **Supp. Fig. 4**), these were not incorporated in the regression.

Wavelength selection: As shown in **Supp. Fig. 5,** 441 nm closely aligns with the absorption peaks of the reduced forms of cIII, cIV, and hemoglobin, thereby enhancing sensitivity to their reduced states. Although our study focuses on the reperfusion phase, when mitochondria and ETC components are predominantly oxidized, accurate detection of their reduced states remains critical for calculating redox status using the 3RMR ratio: reduced / (reduced + oxidized). Because reduced forms are less abundant during oxygenated reperfusion phase, selecting a wavelength that preferentially excites them ensures sufficient signal strength to detect even subtle redox shifts in mitochondrial and ETC complexes.

Data Analysis

During a measurement, scattered light is collected by the probe, where a band pass filter removes the laser wavelength leaving the inelastically scattered photons to be analyzed by the spectrometer. The CCD collects a 2D image of the signal, which is read once per second, with one region of the CCD capturing signal from the liver tissue and another from an internal acetaminophen reference. The location of the acetaminophen peaks is used to shift the measured spectrum to account for changes due to temperature or instrument variations over time. Hot pixels and cosmic rays are subtracted from the image based on a large deviation from the surrounding pixels. The 2D images collapsed to 1D spectra, which are continually averaged together for 180 seconds.

Over the range of baseline analysis (550 cm^{-1}-1750cm^{-1}) a slow varying function (5^{th} order polynomial) is fit to the spectrum to approximate the signal fluorescence. This background is subtracted to form the initial RRS spectrum (y_m) shown in **Fig. 1a**. To refine the baseline estimated during the regression, a baseline refinement is iteratively performed to isolate the sharp RRS peaks from the slower varying fluorescence background. After each iteration of the regression, a cubic spline function is fit to the residual with the resulting baseline estimate subtracted from the RRS spectrum before the next iteration.

T linear regression is performed over a range of 700 cm^{-1} - 1500 cm^{-1} to generate a best fit curve (y_r) which represents the sum of the regression coefficients for the library chromophores times the library spectra. For the liver tissue, we used a library consisting of previously obtained spectra of cIII/cIV or whole mitochondria in both oxidized and reduced states, as described above. Since mitochondrial complexes have resonance maxima of reduced form closer to the excitation wavelength of 441 nm than that of oxidized form (**Supp. Fig. 5**), a unique enhancement factor pair was assigned to each analyte to counterbalance their difference in Soret absorption strength (also shown as f_n in **Fig. 1b**). In specific, reduced / oxidized enhancement factors of our library spectra are 0.15 / 1 for whole mitochondria, 0.28 / 1.4 for cIII, 0.15 /1 for cIV, and 0.17/1 for hemoglobin. Each coefficient (β_n) is multiplied by these enhancement factor (f_n) to account for their relative resonance enhancement, resulting in an adjusted coefficient value that is later used to represent the relative concentration of each chromophore in the tissue. The redox state of each cytochrome complex can be calculated as the ratio of the reduced concentration divided by the sum of the oxidized and reduced concentrations.

Hence, as illustrated in **Fig. 1**, the 3RMR values (%) are calculated as follows: $3RMR\_mito = f_1\beta_1/(f_1\beta_1 + f_2\beta_2)$; $3RMR\_CIII = f_3\beta_3/(f_3\beta_3 + f_4\beta_4)$; $3RMR\_CIV = f_5\beta_5/(f_5\beta_5 + f_6\beta_6)$. In addition, the RRS device also provides oxygen saturation (%) values calculated as $StO_2 = f_8\beta_8/(f_7\beta_7 + f_8\beta_8)$ when hemoglobin or other heme-based oxygen carriers are present. Additionally, the residual spectrum, calculated as $y_m - y_r$ = residual, is minimized to achieve a high quality of the fitting libraries. The root mean square of the residual spectrum (RMS_{error}) is calculated and compared to the estimated shot noise from the CCD, where an RMS_{error} close to the shot noise indicates that the residual is random noise rather than systematic. This ensures that the unexplained spectrum is not from unknown chromophores [18]. Finally, at least 10% of the total signal is mitochondrial specific, thereby ensuring we have enough signal strength to detect the most subtle spectral features to promote accurate identification/quantification.

Liver Viability Assessment

Perfusate Measurements

Inflow and outflow samples were analyzed every 30 minutes with Siemens Rapid-Point 500 (Siemens, Munich, Germany) to primarily monitor pH, pO2 (mmHg), lactate concentration (mmol/mL), and other ion concentrations. Concurrently, flow rate (mL/min) and pressure (mmHg) were recorded and used to calculate vascular resistance as pressure / flow rate / liver weight. Outflow samples were also used to measure hepatic injury markers (AST and ALT) using Activity Assay Kit (Cayman Chemical, Ann Arbor, MI, USA) and cellular apoptosis marker (Cytochrome C) using ELISA Kit (Abcam, USA). The produced bile was collected in Eppendorf tubes and was measured in milliliter (mL) at the end of perfusion. Liver weight was recorded before and after perfusion to determine the weight change. Oxygen consumption (μLO_2 / min per g) was calculated as following: [O_2 solubility coefficient (μL O2 /mL per mmHg)] x [portal vein partial oxygen pressure (mmHg) – vena cava partial oxygen pressure (mmHg)] x portal vein flow (mL/min) / liver weight (g) + [HBOC concentration (g/dL)/100] x HBOC oxygen binding capacity (μL O_2/g) x [(portal vein oxygen saturation – vena cava oxygen saturation)/100] x portal vein flow (mL/min) / liver weight (g). HBOC concentration for 25% v/v was determined to be 3.25 g/dL and HBOC oxygen binding capacity is 1.39 mL O_2/g (provided by Hemoglobin Oxygen Therapeutics, Souderton, PA).

Histological Imaging

Wedge biopsies were fixed in 10% formalin and moved to 70% ethanol after 24 hours. Then, they are processed by the Histology Molecular Pathology Core of Massachusetts General Hospital and Harvard Medical School as previously described [29]. In brief, sections were stained using Dako EnVision+ System-HRP (Dako, Carpinteria, CA, USA). H&E (hematoxylin and eosin) staining was used for vasculature and tissue edema visualization. TUNEL (terminal deoxynucleotidyl transferase dUTP nick end labeling) staining was used to visualize apoptosis. Slides were mounted with the ProLong Glass Antifade Mountant (Thermo Fisher Scientific, USA) and finally scanned at 20× magnification for imaging.

Evaluation of Liver Energy Status

The tissue samples for measurement of bioenergetic molecules were taken at the end of perfusion, immediately flash-frozen in liquid nitrogen, and were stored at -80°C. Then, liquid chromatography-mass spectroscopy (LC-MS) was performed by Mass Spectrometry Core Facility at Shriners Hospital (Boston MA, USA) as previously described [48]. Briefly, crushed tissue biopsies (~25 mg) were dissolved in 250 µL of a 2:1 (v/v) methanol/chloroform mixture and subjected to multiple freeze–thaw cycles. Samples were then analyzed using a 3200 QTRAP LC–MS/MS system (AB Sciex, Foster City, CA) to quantify adenylate energy charge and NAD/NADH ratio. For rat liver samples, ATP concentrations were also obtained from the LC–MS analysis. For pig liver samples, ATP concentrations were measured using the CellTiter-Glo Luminescent Cell Viability Assay (Promega, Madison, WI, USA). Briefly, the CellTiter-Glo reagent was mixed with

ARTICLE IN PRESS

crushed tissue biopsies to generate assay samples and with ATP powder (Sigma-Aldrich, St. Louis, MO, USA) to prepare standards in a 96-well plate. After a 10 min incubation at room temperature, bioluminescence was recorded. In addition, total protein content was quantified using the Pierce™ BCA Protein Assay Kit with Dilution-Free™ BSA Protein Standards (Thermo Fisher Scientific, USA) and used to normalize ATP concentrations.

Statistics and Reproducibility

Experiments were designed with a minimum of n=3 per study group to allow for statistical analysis, and up to n=6 per group enhance experimental reliability. Measurements from different livers were used to produce replicates for statistical comparisons. Unless otherwise stated in the figure legends, no animals were excluded during experiments and analysis. In cases where data points were unavailable and/or excluded, the rationales and updated details are provided in the figure legends. Livers were allocated to groups based on availability and matching of ischemic times rather than formal randomization sequence due to logistical constraints of organ procurement. In addition, animals were housed in the same location and received identical care protocols to minimize potential confounders related to husbandry. To minimize bias from other potential confounders, experiments were performed under comparable environmental and operator conditions to ensure consistency. Blinding was not performed because the experimental setup required knowledge of group allocation during machine perfusion and data collection. All personnel were therefore aware of group allocation throughout the experiment and analysis.

In this study, the primary outcome measure was the use of 3RMR values to differentiate viable from non-viable warm ischemic rat livers after SNMP (1h WI vs 3h WI groups), establishing 3RMR values as indicators of whole-organ viability. Conventional whole-organ parameters (flow rate, oxygen consumption and outflow lactate concentration) were monitored as reference measures consistent with current practice for mitochondrial function and liver viability assessment during *ex vivo* machine perfusion. Combinations of these measures (3RMR, flow rate, oxygen, lactate values) were used to assess therapeutic effectiveness of MB treatment in both rat and pig livers. Additional data, including other perfusate measurements (e.g., AST, ALT, cytochrome C), histological imaging, and liver energy status were used supplementarily to provide a more comprehensive understanding of liver viability and therapeutic effects. Although no specific outcome measures were used to determine sample sizes, n=6 per study group was selected for the primary outcome measures to increase statistical confidence, with fresh liver controls (n=6) were included to confirm that 1h WI livers had function comparable to ideal conditions.

GraphPad PRISM 9 software and Microsoft excel were used to perform graphing and statistical analysis. In the text, data are represented as median (Interquartile range, IQR). In figures, data are shown as bar graphs of median with IQR indicated by error bars, along with scatter dot-plots of individual data points. For study groups with n=3, the IQR is equivalent to the minimum-maximum range. Statistical significance at each time-point was assessed using an unpaired two-tailed Student's T-test with Welch's correction to account for potentially unequal variances. Normality was assumed based on prior experience with these measurements but was not formally tested due to the study small sample sizes (n=3-6). Significantly different comparisons between the two study groups are as indicated in the figure legends. Two-tailed statistical significance was set at $p < 0.05$ unless other denotations for groups are indicated. For evaluating the primary outcome (3RMR values between viable and non-viable warm ischemic rat livers), estimates of effect sizes (differences in mean values between two study groups), with corresponding 95% confidence intervals (CI) and Cohen's d values, were also reported to complement hypothesis testing.

Data availability

ARTICLE IN PRESS

All data relevant to this study are included in this published article and its supplementary material file. Additional information can be provided by the corresponding author upon reasonable request. Source data underlying figures 1-5 can be accessed from Supplementary Data 1.

ARTICLE IN PRESS

ARTICLE IN PRESS

Results

Spectroscopic quantification of mitochondrial redox states

Here, we leverage an *in situ* RRS system to quantify mitochondrial redox state with expanded features to include complexes III and IV (cIII, cIV), as shown in **Fig. 1** (and **Supp. Fig. 2-3**). We focus on cIII and cIV since both are rich in heme groups with resonant Soret band absorption in the ~430–450 nm range [41, 42], which overlaps with our 441 nm excitation wavelength. These properties result in their strong and spectrally distinct Raman signals, as shown in **Supp. Fig. 2**. In contrast, complex I (cI) is not Raman-active under our conditions due to the absence of a heme group [43, 44]. While complex II (cII) may be Raman active with a Soret peak of 416/426 [45], it is present at relatively lower concentrations, as compared to cIII [46], and hence was not captured in the present study.

The RRS system uses a non-contact optical laser probe with an excitation wavelength of 441 nm on the organ surface and records the raw RR spectrum, which is subjected to non-specific background subtraction followed by spectral analysis (**Fig. 1a**). In this approach, we use a regression algorithm to explain the measured RR spectrum (y_m) as a weighted sum (y_r equation) of pre-recorded library RR spectra from isolated, purified analytes such as entire mitochondria, ETC cIII and cIV, as well as hemoglobin (or hemoglobin-based oxygen carrier, HBOC) in both reduced and oxidized states (**Fig. 1b**). MB was confirmed to have non-significant spectroscopic Raman resonance with 441 nm excitation wavelength (**Supp. Fig. 4**). Leveraging spectral differences, the 3RMR values are spectroscopically quantified using regression coefficients of corresponding relevant components in the weighted sum y_r equation. Specifically, the 3RMR_mito is calculated by $f_1\beta_1/(f_1\beta_1 + f_2\beta_2)$ ratio, of which $f_1\beta_1$ is the coefficient (β) adjusted with enhancement factor (f) of reduced mitochondria spectrum (x_1) and $f_2\beta_2$ is the corresponding coefficient adjusted with enhancement factor of oxidized mitochondria spectrum (x_2). The 3RMR_CIII and 3RMR_CIV are also determined using this mathematical approach (**Fig. 1b**). Finally, **Supp. Fig. 5** illustrates the justification for the use of a 441 nm wavelength, which was based on the Soret absorption maxima of key mitochondrial components (cIII and cIV).

Detection of hyperoxidation in rat livers with IRI during machine perfusion

The 3RMR_mito values can range from 0% (completely oxidized) to 100% (completely reduced) in correspondence with various physiological and pathophysiological conditions (**Fig. 2b**). During the optimal reperfusion of healthy rat organs, 3RMR_mito measures have been shown to be consistently stable within a range of low values (10-30%), reflecting a predominantly oxidized state for the entire mitochondria during optimal reperfusion protocol [16-18]. The 3RMR_mito values that exceed this range, therefore, typically indicate various degrees of deoxygenation or ischemia driven by electron accumulation within the ETC complexes. In contrast, the 3RMR_mito values below the optimal range may suggest hyperoxidation, with one potential mechanism due to electron leaks out of the ETC complexes, as illustrated in **Fig. 2c**.

Based on validated DCD rat livers [27], our experiment included three study groups (n=6 per group): fresh livers without WI time, transplantable livers with short 1h WI time, and non-viable livers with prolonged 3h WI time (**Fig. 2a**). Through visual inspection alone, the 3h WI livers exhibit evident signs of IRI after 3 hours of SNMP, characterized by a notable pale appearance (**Fig 2d**). This is confirmed by other perfusion-based parameters, such as increased vascular resistance and weight gain, elevated concentrations of aspartate transaminase (AST) and alanine aminotransferase (ALT), and absent bile production during SNMP (**Supp. Fig. 6**). Further, NAD:NADH ratio and ATP concentration in 3h WI are not recoverable after SNMP (**Supp. Fig. 6f,i**), demonstrating the severity of injury to these livers, as compared to our previous work, whereby SNMP with human livers lead to some improvements in energetic cofactors albeit with

less total ischemic time [48]. Nonetheless, since SNMP alone cannot recover 3h WI livers, this provides an opportunity to leverage this condition to determine therapeutic effectiveness. Like metabolic disruption in livers with cold ischemia [16], electrons accumulate during WI period (high 3RMR) for 1h and 3h WI livers, which is also shown here at T=0 mins in **Fig. 2e**. Immediately after reperfusion, the 3RMR_mito values rapidly drop to less than 20% after 10 mins of SNMP, indicating the effects of re-oxygenation. With more reperfusion time, however, the 3RMR_mito values of 3h WI livers get significantly lower than those in fresh and 1h WI livers, which reach statistically significant after 30 mins in both cases, suggesting a progressive hyperoxidized redox state. At 180 mins of SNMP, 3RMR_mito values are below 10% in 3h WI livers, with an effect size of −9% (95% CI: –11.75% to –6.26%, Cohen's d=−4.46) compared to fresh livers and −7.33% (95% CI: −10.12% to −4.546%, Cohen's d=−3.52) compared to 1h WI livers.

Furthermore, we can derive insights about the exact site of IRI-mediated hyperoxidation using our advanced technology. First, the 3RMR_CIII values are significantly lower in 3h WI livers than in fresh and 1h WI livers ($p<0.05$ at all time-points from T=10 mins onwards) (**Fig. 2f**), and the 3RMR_CIII values in 3h WI livers of 3h WI livers remarkably decrease from 20 (20-23.75)% at T=10 mins to 8 (3.75-12.25)% at T=180 minutes (n=6 per time-point, $p<0.05$). At 180 mins of SNMP, 3RMR_CIII values are statistically lowered in 3h WI livers, with an effect size of −24.33% (95% CI: –32.75 to –15.91, Cohen's d=−3.81) compared to fresh livers and −21% (95% CI: −26.58 to −15.42, Cohen's d=−4.91) compared to 1h WI livers. These results show that hyperoxidization of cIII (effect size over 20% between viable and non-viable liver groups at 180 mins) is much more severe than that of the overall mitochondria (effect size less than 10% at 180 mins), suggesting that cIII is a particularly vulnerable site of injury during reperfusion time. Second, we find no difference in the redox states of cIV among the three liver groups, and the 3RMR_CIV values are zero (completely oxidized) during SNMP (**Fig. 2g**). This 3RMR_CIV result, when considered alone, indicates sufficient oxygen supply to cIV in non-viable 3h WI livers, which contradicts the overall interpretation of other perfusion parameters, that is the 3h WI livers had very restricted oxygen delivery and poor aerobic metabolism. Compared to fresh livers, the 3h WI livers have 50% slower flow rate of perfusate delivering oxygen (**Fig. 2h**), decreased oxygen consumption (**Fig. 2i**), elevated lactate concentration (**Fig. 2j**), reduced mitochondrial energy charge (**Fig. 2k**), and excessive cell death evident in TUNEL imaging (**Fig. 2l**). However, when considering our finding that 3h WI livers have hyperoxidized cIII and overall hyperoxidized mitochondria, the corresponding 3RMR_CIV measures become more understandable. We propose that in 3h WI livers this hyperoxidation is driven by premature electron leaks from cIII, thereby significantly reducing electron transfer to cIV, allowing the limited oxygen supply (from 50% perfusate flow rate) to suffice for electron transfer out of cIV (oxidation). This prevents electron accumulation and reduction in cIV, which would otherwise increase 3RMR_CIV values under similar oxygen-limited conditions.

To further interrogate the potential mechanism underlying this hyperoxidized state, which we hypothesize is due to electron leakiness at cIII, we developed an oxygen stress test (OST). During the OST, livers are transitioned from continuous oxygenated perfusion (i.e., SNMP) to acute ischemia by stopping both perfusate flow and oxygen delivery, leading to an additional period of ischemia (**Fig. 3**). This stress test is based on the principle that if electrons are leaking from mitochondria, then they would display a slower rise in 3RMR (and hence less electron accumulation) with additional ischemia time. Indeed, after the same 3 mins of ischemia introduced at 90 mins of SNMP, the 3RMR_mito of 3h WI livers only reaches 18.64 (17.07 – 22.41) % while 3RMR_mito of fresh and 1h WI livers are 57.07 (45.7 – 65.56) % and 63.59 (56.68 – 66.7) % respectively (n=3 per group, $p<0.05$ fresh vs 3h WI livers & 1h WI vs 3h WI livers). In other words, the average rate of change in 3RMR_mito values is less than 4%/min in 3h WI livers but more than 15%/min in fresh and 1h WI livers.

To further characterize and validate this pathological oxidation within the ETC, we investigated the effects of antimycin A (AA), a well-characterized cIII inhibitor known to increase ROS production at this site [49]. As shown in **Supp. Fig. 7a,** we introduced the study group called

ARTICLE IN PRESS

Fresh + Antimycin A (Fresh+AA). These rat livers did not undergo WI but instead received a dose of AA at a concentration of ~0.02 mM during SNMP. Following AA administration, oxygen consumption in the liver declines significantly and approaches zero by 90 minutes, despite uninterrupted delivery of well-oxygenated perfusate (**Supp. Fig. 7b**). Then, livers underwent OST, and the RRS device was used to measure corresponding shifts in mitochondrial redox states (**Supp. Fig. 7c-g**). The results showed that both fresh and 1h WI livers (>90% transplantable [50]) demonstrates rapid redox transitions, reaching approximately 60% for 3RMR_mito values within just 3 minutes of ischemia onset (**Fig. 3d**). In contrast, 3h WI livers reach only ~20% over the same period (**Fig. 3d**). Notably, the Fresh+AA livers exhibit a redox response during OST that resembled the impaired pattern seen in 3h WI livers (**Supp. Fig. 7c-d**). Finally, **Supp. Fig. 7e-g** shows the 3RMR_mito, 3RMR_CIII, and 3RMR_CIV throughout the full duration of the OST. Interestingly, only the 3RMR of cIV trends differently between 3h WI and Fresh+AA livers, whereby livers exposed to AA remain completely oxidized throughout the OST. This may suggest complete blockage of electron transfer during AA exposure, which is consistent with its mechanisms of action. Taken together, the combination of OST and AA supports our central finding that mitochondrial dysfunction, specifically characterized by pathological oxidation within the ETC, can be readily detected and quantified by our RRS device.

Intervention with methylene blue to rescue mitochondria from WI-induced IRI development

Armed with the knowledge of IRI-mediated hyperoxidation at cIII in 3h WI livers, we investigated the utility of MB which shuttles electrons directly from cI to cytochrome c [28]. We hypothesized that by using MB to bypass cIII during the mitochondrial respiration process, cIV would receive more electrons for consumption of molecular oxygen and livers could be rescued from IRI-mediated mitochondrial injury (**Fig. 4a-b**). Besides treatment with MB alone, we also tested the effects of MB with artificial hemoglobin-based oxygen carriers (HBOC), which is expected to enhance oxygen delivery [51].

The RRS assessment supports our hypothesis with promising outcomes from MB intervention. The 3RMR_mito values trends higher with MB treatment, although statistically non-significantly compared to non-treated 3h WI livers (**Fig. 4c**). In addition, the 3h WI+MB livers had 3RMR_CIII values drop to almost zero (fully oxidized) throughout SNMP (**Fig. 4d**), while their corresponding 3RMR_CIV values increase up to 30% (**Fig. 4e**). These results confirm that MB has effectively altered the electron transfer process to bypass cIII, leaving it without electron deposition from upstream complexes and thus fully oxidized, while improving electron deposition to cIV. The reduced state of cIV in 3h WI+MB livers also inferred that the demand from more electron deposition exceeded oxygen supply from the current SNMP protocol, whose perfusate flow rate does not improve compared to that of 3h WI livers without treatment (**Fig. 4f**), thereby justifying the purpose of the hemoglobin-based oxygen carriers (HBOC). However, it should be noted that while our previous work has shown mitochondrial measurements by RRS in the presence of packed Red Blood Cells (RBCs) and whole blood are feasible [17, 18], the HBOC used in the present study significantly lowered the mitochondrial signal strength. As a result, we were not able to quantify the 3RMR values for the 3h WI+MB+HBOC liver group.

The positive effects of MB in preventing IRI-mediated injury are also observed with other organ viability biomarkers. Oxygen consumption trends higher in 3h WI+MB+HBOC liver groups than in non-treated 3h WI livers, and statistical significance are observed at T= 90 mins ($p=0.0054$) and T=150 mins ($p=0.0468$) (**Fig. 4g**). Lactate outflow concentration trends lower in 3h WI+MB livers (with $p=0.0384$ at T=120 mins) and are statistically lower in 3h WI+MB+HBOC livers than in non-treated 3h WI livers at all time-points except T=10 mins (**Fig. 4h**). Interestingly, compared to fresh liver group, lactate concentration is non-significantly different ($p>0.05$) at T=10, 30 and 180 mins for 3h WI+MB livers; and at all time-points except T=60 mins for 3h WI+MB+HBOC. The observation that lactate concentration of non-viable 3h WI livers is close to physiological baseline highlighted that MB could enhance aerobic respiration. The additional boost of improvement for oxygen consumption, outflow lactate concentration and mitochondrial

ARTICLE IN PRESS

energy charge (**Fig. 4g-i**) in 3h WI+MB+HBOC livers also suggests that HBOC provided some synergistic benefits to the therapeutic cocktail. However, the persistent challenge of suboptimal oxygen delivery due to low perfusate flow rate has hindered many other potential avenues of recovery including weight gain (**Fig. 4j**), cell death (**Fig. 4k**), and other aspects of liver IRI. (**Supp. Fig. 8**).

Translating perfusion-based MB intervention to pig model of DCD livers

Following the demonstration of improved outcomes using MB-supplemented machine perfusion for rat liver models, we proceeded to test the same perfusion-based intervention with pig livers (**Fig. 5a**), comparing fresh control DBD (donation after brain death) livers without WI (Fresh DBD control, n=4), DCD (donation after circulatory death) livers with 30 minutes of WI without treatment (DCD 30min WI, n=4), DCD livers with 30 minutes of WI livers treated with MB+HBOC (DCD 30min WI+MB+HBOC, n=5), and 45 min WI livers treated with MB alone (DCD 45min WI+MB, n=4). These groups were selected since DBD livers are the primary source of livers for transplantation and serve as a reference for optimal graft quality in the absence of WI. Further, the clinical cut-off for WI time in liver transplantation is ≤ 30 mins, whereby ischemic times above this are considered non-transplantable. As such, an untreated 30-minute WI group was included to define the marginal viability threshold, while the 30-minute WI group treated with MB+HBOC was included to define the combined therapeutic effectiveness of both methylene blue and the hemoglobin-based oxygen carrier. Finally, a 45min WI+MB group was included since the ability to rescue livers with greater than 30 min WI time would significantly increase the donor pool of organs. We treated these livers with MB alone since it specifically targets the hyperoxidation of cIII and hence was hypothesized to have the main therapeutic advantage.

Representative livers from each study group by the end of SNMP are shown in **Fig. 5b**. Fresh DBD livers displayed a uniform brownish surface, consistent with healthy tissue. In contrast, 30min WI livers exhibit patchy areas of paler color, indicating mild injury. The 30min WI+MB+HBOC group appears red in color, as the HBOC component dominates the visual appearance and masks the blue hue of MB. The 45min WI+MB livers show a distinct blue coloration due to MB staining. Consistent with these images, fresh DBD controls show values in the healthy 3RMR_mito range (**Fig. 5c**), as observed with rat livers herein and in our other studies [16, 17]. Additionally, within the initial 10 mins of SNMP, RRS assessment shows that both 30min WI livers and 45min WI+MB liver groups had a marked decrease in 3RMR_mito values, reflecting the shift from ischemia to oxygenated reperfusion as seen with rat livers. For the rest of SNMP time, 3RMR_mito values are predominantly less than 10% in 30min WI livers, indicating mitochondrial hyperoxidization. The 3RMR_mito values of 45min WI+MB livers also trends consistently low between zero to 5%, but this is an expected result considering MB therapeutic effects. In specific, as shown in rat livers, MB makes cIII fully oxidized (**Fig. 4d**) instead of restoring its regular 30-35% reduced state (**Fig. 2f**), and if oxygen delivery is improved for sufficient electron transfer at cIV, this complex would also become fully oxidized (**Fig. 2g**), which together can lead to an artificially hyperoxidized state of the entire mitochondria under MB treatment. Hemodynamic results suggest that MB-treated livers were likely to benefit from higher oxygen delivery. Compared to 30mins WI livers, portal flow rate increases 2-fold in 30mins WI+MB+HBOC livers and almost 4-fold in 45mins WI+MB livers (**Fig. 5d**, $p<0.05$ at all time-points for both treated liver groups in comparison to 30min WI livers, except T=180 min for 45mins WI+MB). Portal vascular resistance trends lower in 30mins WI+MB+HBOC livers (although $p>0.05$, except at T=10 min) and significantly decreased in 45mins WI+MB livers in comparison to non-treated WI livers (**Fig. 5e**, $p<0.05$ at all time-points except T=30 min). Further, MB improved aerobic respiration during SNMP. The 30mins WI+MB+HBOC livers exhibit a 2-fold higher oxygen consumption (**Fig. 5f**, $p<0.05$ at T=30, 60, 90, 150, 180 mins) and a trend of lower lactate outflow concentration although non-significant statistically (**Fig. 5g**) than non-treated WI livers. In addition, the 45mins WI+MB livers consume as much oxygen as the 30mins WI+MB+HBOC livers (**Fig. 5f**), with even a lower trend of lactate outflow concentration (**Fig. 5g**, $p<0.05$ at all time-points except T=10 min, 45mins

ARTICLE IN PRESS

WI+MB vs 30mins WI livers). Potassium outflow concentration, a liver injury biomarker, continuously decreases throughout reperfusion time for all three liver groups (**Fig. 5h**), thus showing the overall benefits of SNMP for DCD liver functional recovery. Perhaps the most important outcome is the striking similarities between Fresh DBD and DCD 45min WI+MB livers, whereby there are no significant differences in hemodynamics and oxygen/lactate values, demonstrating the potential of methylene blue to recover the function of livers exposed to severe WI (**Fig. 5d-g**). Nonetheless, it should be noted that 3RMR_mito at T=60 (**Fig. 5c**), and select injury markers at select time points are significantly different comparing Fresh DBD and 45 min WI+MB livers, including concentrations of potassium at T=30 min (**Fig. 5h**), AST at T=180 min (**Supp. Fig. 9a**), and cytochrome c at T=120 min (**Supp. Fig. 9c**). In addition, 45mins WI+MB livers show more favorable recovering trends than 30mins WI+MB+HBOC in many parameters such as portal flow rate, resistance, oxygen consumption, as well as lactate and ATP concentrations **(Fig 5d-g; Supp. Fig. 9f)**, suggesting that HBOC may not be an optimal oxygen carrier to pair with MB treatment.

Taken together, these results indicate potential for the clinical translation of this perfusion-based MB intervention to improve the recovery of human DCD livers that are currently considered marginal with extended WI durations. Additionally, because MB directly alleviates dysfunction at cIII, its effectiveness in recovering the whole-organ oxygen/lactate values provides functional confirmation that hyperoxidation at cIII drives liver warm ischemia-reperfusion injury development. They also showcase the usefulness of this *in situ* RRS technology for fundamental scientific endeavors that can help develop effective targeted therapeutic intervention for the perfusion/recovery of DCD livers with extended WI time.

ARTICLE IN PRESS

Discussion

Here, we present an innovation using our RRS technique to detect IRI-mediated mitochondrial injury in livers during machine perfusion, and to evaluate mitochondria-targeted therapeutics such as MB. As compared to other methods that require complicated and/or time-consuming tissue sampling and mitochondrial isolations, our RRS system can provide non-destructive label-free measurements, while collecting the redox states of whole mitochondria and individual complexes in the ETC, including cIII and cIV (**Fig. 1, Supp. Fig. 1-2**). We show that our RRS system can be used both for individual time-point evaluation during machine perfusion time (**Fig. 2**), and for continuous monitoring of dynamic changes during an oxygen stress test (**Fig. 3**). Taken together, this illustrates the versatility of our RRS approach that can be easily adapted to assess IRI-mediated mitochondrial injury in other tissues or organs.

We demonstrate the potential of our RRS technology in solving complex biological problems by using the RRS assessment to elucidate WI-induced mitochondrial injury pathway in liver IRI development, a multi-factorial problem that is detrimental to clinical outcomes of DCD liver transplants [52, 53]. Our initial observation centers on a decrease in the 3RMR_CIII as a function of perfusion from rat livers exposed to 3 hours of WI (3h WI; **Fig. 2f**, red line), indicating a progression towards a hyperoxidized state. This was matched with biochemical results to confirm increased stress in the 3h WI liver group, including reduced oxygen consumption (**Fig. 2i**), elevated lactate concentration (**Fig. 2j**), decreased energy charge (**Fig. 2k**), visible cell death (as shown by TUNEL staining; **Fig. 2l**), elevated concentrations of AST and ALT (**Supp. Fig. 5b-c**), and the release of cytochrome c into the perfusate (**Supp. Fig. 5e**). To interrogate the potential mechanism underlying hyperoxidation at cIII, we used several experimental approaches, including the oxygen stress test (OST) and therapeutic interventions (with methylene blue, MB, and antimycin A, AA). During OST, perfused livers were exposed to an additional period of ischemia (defined by a compete pause of both perfusate fluid flow and oxygen air supply for 10 min; **Fig. 3**). This stress test is based on the principle that if electrons leak from mitochondria, then they would display a slower rise in 3RMR with additional ischemia time since they cannot retain electrons required for a higher (more reduced) 3RMR. Indeed, after 3 mins of ischemia introduced at 90 mins of SNMP, the 3RMR_mito of of 3h WI livers only reaches 18.64 (17.07 – 22.41) % while 3RMR_mito of fresh and 1h WI livers are 57.07 (45.7 – 65.56) % and 63.59 (56.68 – 66.7) % respectively (n=3 per group, $p<0.05$ fresh vs 3h WI livers & 1h WI vs 3h WI livers). In other words, the average rate of change in 3RMR_mito values is less than 4%/min in 3h WI livers but more than 15%/min in fresh and 1h WI livers. This also suggests that hyperoxidation in 3h WI livers may be due to electron leakage, although additional evidence is required.

Secondly, we leverage the known mode of action of two therapeutics, including MB and AA. While MB shuttles electrons from cI to cytochrome c (which then transfers to cIV, thereby bypassing cIII), AA is a well-characterized cIII inhibitor known to increase ROS production at this site [49]. Specifically, when 3h WI livers are treated with MB, we observe a decrease in 3RMR_CIII and an increase in 3RMR_CIV (see **Fig. 4d and Fig. 4e**). Although 3RMR values outside of the normal zone (i.e. 12-20%; **Fig. 2b**) are typically associated with mitochondrial stress, in this case, the values reflect the therapeutic action of MB. As noted above, since MB shuttles electrons from cI to cytochrome c, the decrease in 3RMR_CIII (i.e. hyperoxidation) in the presence of MB is evidence that electrons are effectively bypassing cIII. In contrast, the increase in 3RMR_CIV suggests that MB is helpful in depositing electrons to cIV (via cytochrome c), resulting in the rise in 3RMR_CIV (or relatively high reduced state). This relatively high reduced state at CIV may have also been matched with not enough oxygen molecules for electron transfer (**Fig. 4e**). While its possible this is due to suboptimal re-introduction of oxygenated perfusate in current SNMP protocol, it would be interesting to test how gradual re-warming [54, 55] or hypothermic [56, 57] machine perfusion protocols could change this dynamic in further studies. Finally, we investigate the effects of AA, whereby livers from the “Fresh + Antimycin A” (Fresh+AA) group exhibit a redox response during OST that closely mirrored the impaired redox dynamics observed in 3h WI livers

(**Supp. Fig. 6**). The striking similarity in RRS-derived redox shift behavior between the Fresh+AA and 3h WI groups during the OST supports our central finding that mitochondrial dysfunction, specifically characterized by pathological oxidation at cIII within the ETC, plays a key role in driving liver IRI following prolonged WI.

It is important to note that while these therapeutic interventions provide a means to interrogate the underlying mechanism of hyperoxidation at cIII, MB in particular has high translational potential to overcome hyperoxidation at cIII, especially in the liver transplant setting. Indeed, in testing MB for recovering IRI in rat livers, the results demonstrate improved aerobic metabolism, evident by significantly improved lactate concentration and increased oxygen consumption (**Fig. 4g-h**), thereby motivating the translation of MB to a pre-clinical large animal model such as the pig. In pursuit of this goal, perhaps the most important outcomes are the striking similarities between Fresh DBD and 45 min WI+MB pig livers, whereby there are almost no differences in hemodynamics and oxygen/lactate values, demonstrating the potential of MB to recover the function of livers exposed to severe WI (**Fig. 5** and **Supp. Fig. 8**). While this result is striking, the 45min WI+MB group outperformed the 30min WI+MB+HBOC group in portal flow, oxygen consumption, and lactate concentration, indicating that HBOC could be counterproductive in the pig model. While the reason for this outcome requires further investigation, HBOC has been reported to scavenge nitric oxide, leading to vasoconstriction and impaired microcirculation [58-60]. In this capacity, these unintended effects of HBOC can reduce effective tissue perfusion and oxygen delivery at the microvascular level, which is critical for MB to reach and act on injured mitochondria, thus blunting the therapeutic impact of MB. Irrespective of the underlying reason for the counterproductive effects of HBOC, a comparison of the MB+HBOC versus MB alone group further supports our central hypothesis that pathological oxidation within the ETC is a key driver of liver IRI following prolonged WI. Here, we also want to acknowledge that our study has notable limitations, including the small sample sizes (n<10) and reliance on animal models, which may not fully replicate human physiology. These factors should be considered when interpreting the findings.

Overall, our RRS assessment presented here enables the detection of a critical IRI-mediated mitochondrial injury pathway and guides us to an effective mitochondria-targeted therapeutic approach that is scalable from small to large animal models of DCD livers. While we demonstrate the capability of RRS to track mitochondrial injury in acellular perfusates during SNMP with acellular perfusates, our previous work has also shown its ability to measure mitochondrial function during normothermic machine perfusion with RBC-based perfusates [17], thereby demonstrating its translational relevance. However, it should be noted that the present study did observe a decrease in mitochondrial signal strength in the presence of HBOC, thereby prohibiting the tracking of 3RMR in these groups. We anticipate that our findings will spark broad discoveries to increase organ availability. Implementations of our work can be used in studies such as developing therapeutic cocktails for organ mitochondrial preservation, improving machine perfusion protocols to mitigate IRI during DCD organ recovery, and perhaps even establishing an extended clinical criterion to include RRS-derived biomarkers for assessment of other marginal DCD organs with extended WI time prior to transplant. Altogether, we are optimistic that future approaches will leverage the principles presented here to further explore the landscape of emerging solutions to solve ischemia-reperfusion injury far beyond transplantation.

Authors' contributions: K.T.N, O.S.O and S.N.T designed the study. K.T.N and O.S.O. performed the rat liver machine perfusion. C.T and K.T.N performed the pig liver machine perfusion with support from O.S.O and R.J. K.T.N was responsible for resonance Raman Spectroscopy (RRS) data collection and interpretation. O.S.O was responsible for rat and pig liver procurements. K.T.N, O.S.O, C.T, and T.P contributed to organ viability data generation and interpretation. K.T.N., R.J., P.R, contributed to RRS algorithm optimization and data analysis with support from E.A. and D.V additionally. J.N.K, P.R. and D.V contributed to developing the RRS library for individual complex III and IV. K.T.N. performed the data curation, and R.J. performed the statistical hypothesis testing with support from K.T.N., O.S.O., and A.M. Overall, S.N.T. is responsible for all aspect of the research project with support for laboratory resources from K.U, surgical techniques and pig liver resources from S.A.R, A.A.O; as well as engineering support for RRS technology development from D.V. and P.R. All authors reviewed and edited the manuscript.

Acknowledgements: This work was supported by generous funding to S.N.T. from the US National Institutes of Health (R01DK134590). We also gratefully acknowledge funding to S.N.T from the US National Institute of Health (K99/R00 HL1431149; R01HL157803; R24OD034189), National Science Foundation (EEC 1941543), Polsky Family Foundation, and Shriners Children's Boston (Grant #BOS-85115). In addition, we acknowledge fundings to K.U. from the US National Institute of Health (R01DK114506**,** R01DK096075), and support for R.J. by Grant #LIFER23-263034 from the American Association for the Study of Liver Diseases Foundation. This work was also supported by the Office of the Assistant Secretary of Defense for Health Affairs through the Peer Reviewed Medical Research Program under Award Number W81XWH-19-1-0472 to J.N.K. Opinions, interpretations, conclusions, and recommendations are those of the author and are not necessarily endorsed by the Department of Defense. The authors express deep gratitude for expert support from highly skilled technicians of the MGH Knight Surgery for the pig liver procurements, that of Pathology Core from Harvard Medical School for histology studies, and that of Mass Spectroscopy Core from Shriners Hospital for Children – Boston for the liver energy status evaluation. We would like to extend our gratitude to Dr. Robert Balaban and Dr. Armel Femnou from the NIH National Heart, Lung, and Blood Institute for his expertise in mitochondrial energetics and his important assistance in developing the RRS library of individual mitochondrial complexes. In addition, we would like to thank Ms. Jesslyn James from the Xavier University of Louisiana for her support with pig liver machine perfusion and RRS measurements at MGH during a research experience for undergraduate (REU) program funded by the NSF Grant No. EEC 1941543. We would like to thank Dr. Alissa Cutrone and Dr. Arnaud Lyon for their surgical support with pig liver procurement. We also deeply appreciate Dr. Reinier J de Vries and Ms. Casie A. Pendexter for valuable contributions to the human liver experiments. Finally, we express sincere gratitude to Mr. Zafiris Zafirelis and HbO2 Therapeutics for their provision of hemoglobin-based oxygen carrier (HBOC) used in this study.

Conflict of Interest: The authors declare competing interests. S.N.T, J.N.K and P.R. have provisional patent applications relevant to this study. D.V and P.R. are employees and shareholders of Pendar Technologies. S.N.T's are managed by MGH and Partners HealthCare in accordance with their conflict-of-interest policies. J.N.K's competing interests are managed by BCH's conflict-of-interest policies. D.V and P. R.'s competing interests are subject to the Research Integrity Policy of Pendar Technologies. The following patented technologies have been used in this study: US2020/0281474A1 In-vivo monitoring of cellular energetics with Raman spectroscopy (application). Additional patent applications for use in ophthalmology, tissue viability, and burn injury assessment using Resonance Raman Spectroscopy have been submitted where R.J. is also an inventor. Finally, a patent disclosure was submitted for the use of methylene blue to overcome ischemia-reperfusion injury where K.T.N, O.S.O and S.N.T are co-inventors. This does

ARTICLE IN PRESS

not alter our adherence to journal policies on sharing data and materials. All other authors do not have competing interests.

ARTICLE IN PRESS

References

1. Brand, M.D., et al., *The role of mitochondrial function and cellular bioenergetics in ageing and disease.* Br J Dermatol, 2013. **169 Suppl 2**(0 2): p. 1-8.
2. Jastroch, M., et al., *Mitochondrial proton and electron leaks.* Essays Biochem, 2010. **47**: p. 53-67.
3. Mazat, J.P., A. Devin, and S. Ransac, *Modelling mitochondrial ROS production by the respiratory chain.* Cell Mol Life Sci, 2020. **77**(3): p. 455-465.
4. Bardaweel, S.K., et al., *Reactive Oxygen Species: the Dual Role in Physiological and Pathological Conditions of the Human Body.* Eurasian J Med, 2018. **50**(3): p. 193-201.
5. Fromenty, B. and M. Roden, *Mitochondrial alterations in fatty liver diseases.* J Hepatol, 2023. **78**(2): p. 415-429.
6. Hiran A. Prag, D.K.-A., Timothy E. Beach, Anja V. Gruszczyk, Nils Burger, Michael P. Murphy, *Chapter 26 - Mitochondrial ROS production during ischemia-reperfusion injury*, in *Oxidative Stress*, H. Sies, Editor. 2020, Academic Press. p. 513-538.
7. Schatten, H., Q.Y. Sun, and R. Prather, *The impact of mitochondrial function/dysfunction on IVF and new treatment possibilities for infertility.* Reprod Biol Endocrinol, 2014. **12**: p. 111.
8. Li, J.L., et al., *Mitochondrial Function and Parkinson's Disease: From the Perspective of the Electron Transport Chain.* Front Mol Neurosci, 2021. **14**: p. 797833.
9. Bruinsma, B.G., et al., *Peritransplant Energy Changes and Their Correlation to Outcome After Human Liver Transplantation.* Transplantation, 2017. **101**(7): p. 1637-1644.
10. Eden, J., et al., *Assessment of liver graft quality during hypothermic oxygenated perfusion: The first international validation study.* J Hepatol, 2025. **82**(3): p. 523-534.
11. Logan, A., et al., *Assessing the Mitochondrial Membrane Potential in Cells and In Vivo using Targeted Click Chemistry and Mass Spectrometry.* Cell Metab, 2016. **23**(2): p. 379-85.
12. Sivandzade, F., A. Bhalerao, and L. Cucullo, *Analysis of the Mitochondrial Membrane Potential Using the Cationic JC-1 Dye as a Sensitive Fluorescent Probe.* Bio Protoc, 2019. **9**(1).
13. Meszaros, A.T., et al., *Mitochondrial respiration during normothermic liver machine perfusion predicts clinical outcome.* EBioMedicine, 2022. **85**: p. 104311.
14. Kuznetsov, A.V., et al., *Evaluation of mitochondrial respiratory function in small biopsies of liver.* Anal Biochem, 2002. **305**(2): p. 186-94.
15. Koliaki, C., et al., *Adaptation of hepatic mitochondrial function in humans with non-alcoholic fatty liver is lost in steatohepatitis.* Cell Metab, 2015. **21**(5): p. 739-46.
16. de Vries, R.J., et al., *Non-invasive quantification of the mitochondrial redox state in livers during machine perfusion.* PLoS One, 2021. **16**(10): p. e0258833.
17. Jain, R., et al., *Real-time monitoring of mitochondrial oxygenation during machine perfusion using resonance Raman spectroscopy predicts organ function.* Sci Rep, 2024. **14**(1): p. 7328.
18. Perry, D.A., et al., *Responsive monitoring of mitochondrial redox states in heart muscle predicts impending cardiac arrest.* Sci Transl Med, 2017. **9**(408).
19. Jassem, W. and N.D. Heaton, *The role of mitochondria in ischemia/reperfusion injury in organ transplantation.* Kidney Int, 2004. **66**(2): p. 514-7.
20. Tennankore, K.K., et al., *Prolonged warm ischemia time is associated with graft failure and mortality after kidney transplantation.* Kidney Int, 2016. **89**(3): p. 648-58.
21. Abt, P.L., et al., *Survival following liver transplantation from non-heart-beating donors.* Ann Surg, 2004. **239**(1): p. 87-92.
22. White, C.W., et al., *Transplantation of Hearts Donated after Circulatory Death.* Front Cardiovasc Med, 2018. **5**: p. 8.
23. Eden, J., et al., *Utilization of livers donated after circulatory death for transplantation - An international comparison.* J Hepatol, 2023. **78**(5): p. 1007-1016.

ARTICLE IN PRESS

ARTICLE IN PRESS

24. Beuth, J., et al., *New Strategies to Expand and Optimize Heart Donor Pool: Ex Vivo Heart Perfusion and Donation After Circulatory Death: A Review of Current Research and Future Trends.* Anesth Analg, 2019. **128**(3): p. 406-413.
25. Jawitz, O.K., et al., *Increasing the United States heart transplant donor pool with donation after circulatory death.* J Thorac Cardiovasc Surg, 2020. **159**(5): p. e307-e309.
26. Goldaracena, N., et al., *Expanding the donor pool for liver transplantation with marginal donors.* Int J Surg, 2020. **82S**: p. 30-35.
27. Tolboom, H., et al., *Recovery of warm ischemic rat liver grafts by normothermic extracorporeal perfusion.* Transplantation, 2009. **87**(2): p. 170-7.
28. Xue, H., A. Thaivalappil, and K. Cao, *The Potentials of Methylene Blue as an Anti-Aging Drug.* Cells, 2021. **10**(12).
29. Tessier, S.N., et al., *Partial freezing of rat livers extends preservation time by 5-fold.* Nat Commun, 2022. **13**(1): p. 4008.
30. Chen, M., et al., *Contrast-Enhanced Ultrasound to Quantifyc Perfusion in a Machine-Perfused Pig Liver.* Annu Int Conf IEEE Eng Med Biol Soc, 2018. **2018**: p. 3128-3131.
31. Bruinsma, B.G., et al., *Subnormothermic machine perfusion for ex vivo preservation and recovery of the human liver for transplantation.* Am J Transplant, 2014. **14**(6): p. 1400-9.
32. Olverson, G.t., et al., *Cardiac Loading using Passive Left Atrial Pressurization and Passive Afterload for Graft Assessment.* J Vis Exp, 2024(210).
33. Bruinsma, B.G., et al., *Supercooling preservation and transplantation of the rat liver.* Nat Protoc, 2015. **10**(3): p. 484-94.
34. Shi, Z.F., et al., *Methylene blue ameliorates brain edema in rats with experimental ischemic stroke via inhibiting aquaporin 4 expression.* Acta Pharmacol Sin, 2021. **42**(3): p. 382-392.
35. Xin, J., et al., *Spatial transcriptomics analysis of zone-dependent hepatic ischemia-reperfusion injury murine model.* Commun Biol, 2023. **6**(1): p. 194.
36. Palladini, G., et al., *Lobe-specific heterogeneity and matrix metalloproteinase activation after ischemia/reperfusion injury in rat livers.* Toxicol Pathol, 2012. **40**(5): p. 722-30.
37. Covian, R., et al., *Spectroscopic identification of the catalytic intermediates of cytochrome c oxidase in respiring heart mitochondria.* Biochimica et Biophysica Acta (BBA) - Bioenergetics, 2023. **1864**(2): p. 148934.
38. Glancy, B. and R.S. Balaban, *Protein composition and function of red and white skeletal muscle mitochondria.* Am J Physiol Cell Physiol, 2011. **300**(6): p. C1280-90.
39. Balaban, R.S., V.K. Mootha, and A. Arai, *Spectroscopic determination of cytochrome c oxidase content in tissues containing myoglobin or hemoglobin.* Anal Biochem, 1996. **237**(2): p. 274-8.
40. Ljungdahl, P.O., J.D. Pennoyer, and B.L. Trumpower, *[18] Purification of cytochrome bc1 complexes from phylogenically diverse species by a single method*, in *Methods in Enzymology*. 1986, Academic Press. p. 181-191.
41. Spiro, T.G., *Resonance raman spectroscopic studies of heme proteins.* Biochimica et Biophysica Acta (BBA) - Reviews on Bioenergetics, 1975. **416**(2): p. 169-189.
42. Callahan, P.M. and G.T. Babcock, *Insights into heme structure from soret excitation Raman spectroscopy.* Biochemistry, 1981. **20**(4): p. 952-958.
43. Hinchliffe, P. and L.A. Sazanov, *Organization of iron-sulfur clusters in respiratory complex I.* Science, 2005. **309**(5735): p. 771-4.
44. Baradaran, R., et al., *Crystal structure of the entire respiratory complex I.* Nature, 2013. **494**(7438): p. 443-448.
45. Valyushok, D.S., et al., *Identification of a new b-type cytochrome from the whitefish Coregonidae eggs.* FEBS Letters, 1993. **332**(1-2): p. 61-63.

ARTICLE IN PRESS

ARTICLE IN PRESS

46. Schägger, H. and K. Pfeiffer, *The Ratio of Oxidative Phosphorylation Complexes I–V in Bovine Heart Mitochondria and the Composition of Respiratory Chain Supercomplexes*.* Journal of Biological Chemistry, 2001. **276**(41): p. 37861-37867.
47. Siletsky, S.A. and A.A. Konstantinov, *Cytochrome c oxidase: Charge translocation coupled to single-electron partial steps of the catalytic cycle.* Biochimica et Biophysica Acta (BBA) - Bioenergetics, 2012. **1817**(4): p. 476-488.
48. Bruinsma, B.G., et al., *Metabolic profiling during ex vivo machine perfusion of the human liver.* Sci Rep, 2016. **6**: p. 22415.
49. Ogita, M., et al., *Antimycin A-induced cell death depends on AIF translocation through NO production and PARP activation and is not involved in ROS generation, cytochrome c release and caspase-3 activation in HL-60 cells.* The Journal of Antibiotics, 2009. **62**(3): p. 145-152.
50. Tolboom, H., et al., *Subnormothermic machine perfusion at both 20°C and 30°C recovers ischemic rat livers for successful transplantation.* J Surg Res, 2012. **175**(1): p. 149-56.
51. Aburawi, M.M., et al., *Synthetic hemoglobin-based oxygen carriers are an acceptable alternative for packed red blood cells in normothermic kidney perfusion.* Am J Transplant, 2019. **19**(10): p. 2814-2824.
52. Liu, J. and K. Man, *Mechanistic Insight and Clinical Implications of Ischemia/Reperfusion Injury Post Liver Transplantation.* Cell Mol Gastroenterol Hepatol, 2023. **15**(6): p. 1463-1474.
53. Nemeth, N., et al., *Hemorheological and Microcirculatory Factors in Liver Ischemia-Reperfusion Injury-An Update on Pathophysiology, Molecular Mechanisms and Protective Strategies.* Int J Mol Sci, 2021. **22**(4).
54. Mahboub, P., et al., *Gradual rewarming with a hemoglobin-based oxygen carrier improves viability of donation after circulatory death in rat livers.* Front Transplant, 2024. **3**: p. 1353124.
55. Minor, T., et al., *Controlled oxygenated rewarming as novel end-ischemic therapy for cold stored liver grafts. A randomized controlled trial.* Clin Transl Sci, 2022. **15**(12): p. 2918-2927.
56. van Rijn, R., et al., *Hypothermic Machine Perfusion in Liver Transplantation - A Randomized Trial.* N Engl J Med, 2021. **384**(15): p. 1391-1401.
57. McGiffin, D.C., et al., *Hypothermic oxygenated perfusion (HOPE) safely and effectively extends acceptable donor heart preservation times: Results of the Australian and New Zealand trial.* J Heart Lung Transplant, 2024. **43**(3): p. 485-495.
58. Yu, B., K.D. Bloch, and W.M. Zapol, *Hemoglobin-based red blood cell substitutes and nitric oxide.* Trends Cardiovasc Med, 2009. **19**(3): p. 103-7.
59. Cabrales, P. and J.M. Friedman, *HBOC vasoactivity: interplay between nitric oxide scavenging and capacity to generate bioactive nitric oxide species.* Antioxid Redox Signal, 2013. **18**(17): p. 2284-97.
60. Song, B.K., et al., *Effects of a hemoglobin-based oxygen carrier (HBOC-201) and derivatives with altered oxygen affinity and viscosity on systemic and microcirculatory variables in a top-load rat model.* Microvasc Res, 2014. **95**: p. 124-30.

Figure Legends

Fig. 1: Summary of the RRS data processing and computational pipeline. **(a)** Flow chart of data analysis using NI LabVIEW software. The raw spectrum from a representative rat liver is adjusted to remove cosmic rays and dark current, and the fluorescence baseline is subtracted, leaving the Raman spectrum (y_m). A regression analysis is performed against the library of known spectra to determine the best fit, which represents the relative concentrations of chromophores in the tissue within the Raman shift range of 700 to 1500 cm^{-1} (y_r), and together achieves random residual spectrum of unexplained signal accounting for less than 4% of the measured spectrum (y_m - y_r = residual) **(b)** Libraries of known spectra are created from the purified, isolated analytes, including reduced and oxidized whole mitochondria (x_1, x_2), reduced and oxidized complex III (x_3, x_4), reduced and oxidized complex IV (x_5, x_6), and reduced and oxidized hemoglobin (x_7, x_8). Since mitochondrial complexes have resonance maxima of the reduced form closer to the excitation wavelength of 441 nm than that of oxidized form, a unique enhancement factor pair was assigned to each analyte to counterbalance their difference in Soret absorption strength, resulting in their corresponding adjusted coefficient values (i.e., $f_1\beta_1, f_2\beta_2$ ...). Finally, we show their mathematical relationship that yields 3RMR values.

Fig. 2: RRS detects mitochondrial hyperoxidation during SNMP of rat livers with extended warm ischemia. **(a)** Schematic of experimental design. Rat livers are cannulated and explanted, then exposed to either 0, 1, or 3 hours of warm ischemia (WI) prior to subnormothermic machine perfusion (SNMP). **b)** The range of possible 3RMR_mito values from 0% (fully oxidized) to 100% (fully reduced) with corresponding biological interpretations. **(c)** Schematic of the potential mechanism of the hyperoxidized mitochondrial state, which may be attributed to electron leakiness at complex III. **(d)** Images of fresh (left) and 3h WI (right) rat livers after SNMP, which show evidence of IRI (weight gain, pale color) in 3h WI livers. From RRS assessment, **(e)** 3RMR_mito, **(f)** 3RMR_CIII and **(g)** 3RMR_CIV indicated increasingly hyperoxidized mitochondria and hyperoxidized complex III as a vulnerable site of injury in 3h WI livers. Please note that RRS data at T=0 min (after WI, shortly before SNMP) was not collected for fresh livers because they were reperfused immediately after procurement without WI. During SNMP, **(h)** flow rate, **(i)** oxygen consumption, and **(j)** outflow lactate concentration collectively showed poor aerobic respiration and viability in 3h WI liver. After SNMP, **(k)** mitochondrial energy charge, and **(l)** TUNEL images, with dead cells (brown dots) and relative edema (white space) in images, further confirmed IRI effects in 3h livers. Study was designed with n=6 per group with data presented as median ± interquartile range (IQR). Statistical significance at each time point was assessed using an unpaired two-tailed Student's t-test with Welch's correction, where the following symbols denote $p < 0.05$ for the corresponding comparisons: (#) Fresh vs 1h WI; (*) 1h WI vs 3h WI; (+) Fresh vs 3h WI.

Fig. 3: RRS oxygen stress test interrogates the mechanism of mitochondrial hyperoxidation in 3hWI rat livers. Mechanistically, if hyperoxidation occurs due to electron leakiness, ETC complexes would not be able to accumulate electrons and could not become reduced as quickly in response to ischemia. **(a)** Schematic of the oxygen stress test (OST) method. **(b)** Representative RRS measure spectrum during reperfusion (with O_2) and ischemia (without O_2). **(c)** 3RMR_mito values after 3 mins of ischemia induced by the OST. Study was designed with n=3 per group with data presented as median ± interquartile range (IQR). Statistical significance at each time point was assessed using an unpaired two-tailed Student's t-test with Welch's correction, where the following symbols denote $p < 0.05$ for the corresponding comparisons: (#) Fresh vs 1h WI; (*) 1h WI vs 3h WI; (+) Fresh vs 3h WI. **(d)** Representative trendline of 3RMR_mito values as a function of OST time. After the depletion of oxygen, mitochondria of 3hWI livers become reduced more slowly than that of fresh and 1hWI livers.

Fig. 4: **Methylene Blue mitigates IRI-mediated mitochondrial injury of 3hWI rat livers. (a)** Schematic of MB therapeutic mechanism via bypassing complex III, and HBOC's proposed benefit via increasing oxygen delivery. **(b)** Doses and administration of MB and HBOC during machine perfusion. From RRS measures, **(c)** 3RMR_mito, **(d)** 3RMR_CIII, **(e)** 3RMR_CIV confirmed the MB effects, evident with fully oxidized complex III due to electron transfer bypass and reduced complex IV due to enhanced electron deposition without changes to perfusate flow rate for oxygen supply. Viability biomarkers **(f)** flow rate, **(g)** oxygen consumption, **(h)** outflow lactate concentration. After SNMP, **(i)** mitochondrial energy charge, **(j)** weight gain, and **(k)** TUNEL images showed non-significant differences in cell death (brown dots) and relative tissue edema (white space) between the 3hWI+MB and 3h WI+HBOC livers. Please note that HBOC used in the present study significantly lowered the mitochondrial signal strength, thereby we were not able to quantify 3RMR values for the 3hWI+MB and 3h WI+HBOC liver groups. Study was designed as following: 3h WI (n=6), 3h WI+MB (n=3) and 3h WI+MB+HBOC (n=3); data presented as median ± interquartile range (IQR). Statistical significance at each time point was assessed using an unpaired two-tailed Student's t-test with Welch's correction, where the following symbols denote $p < 0.05$ for the corresponding comparisons: (#) 3h WI vs 3h WI+MB; (*) 3h WI+MB vs 3h WI+MB+HBOC; (+) 3h WI vs 3h WI+MB+HBOC.

Fig. 5: Methylene Blue improves hemodynamics and aerobic metabolism of DCD pig livers. **(a)** Schematic showing timeline of procurement, treatment, and measurements. After SNMP, **(b)** images of DCD livers representative of each study group. During SNMP, **(c)** 3RMR_mito, **(d)** portal flow rate, **(e)** portal vascular resistance, **(f)** oxygen consumption, **(g)** outflow lactate concentration, and **(h)** outflow potassium concentration. Please note that HBOC used in the present study significantly lowered the mitochondrial signal strength, thereby we were not able to quantify the 3RMR values for the 30 min WI+MB+HBOC liver group. Study was designed as following: 30 min WI (n=4), 30 min WI+MB+HBOC (n=5), 45 min WI+MB (n=4) and Fresh DBD (n=4); data presented as median ± interquartile range (IQR). Statistical significance at each time point was assessed using an unpaired two-tailed Student's t-test with Welch's correction, where the following symbols denote $p < 0.05$ for the corresponding comparisons: (*) 30 min WI vs 30 min WI+MB+HBOC; (#) 30 min WI vs 45 min WI+MB; (+) 30 min WI+MB+HBOC vs 45 min WI+MB; (†) 30 min WI vs Fresh DBD; (Ω) 30 min WI+MB+HBOC vs Fresh DBD; (β) 45 mins WI+MB vs Fresh DBD.

ARTICLE IN PRESS

ED Summary:

Nguyen, Ozgur et al. applied resonance Raman Spectroscopy (RRS) to monitor mitochondrial redox states in rat and pig livers during reperfusion after warm ischemia, including resolving redox changes at complexes III and IV. RRS detects early mitochondrial hyperoxidation, particularly at complex III and that RRS guided treatment with methylene blue can restore function in injured livers, highlighting its potential for improving organ assessment and rescue in transplantation.

Peer review information: *Communications Medicine* thanks Oner Ulger, Kosuke Dodo and the other, anonymous, reviewer(s) for their contribution to the peer review of this work.

ARTICLE IN PRESS

ARTICLE IN PRESS

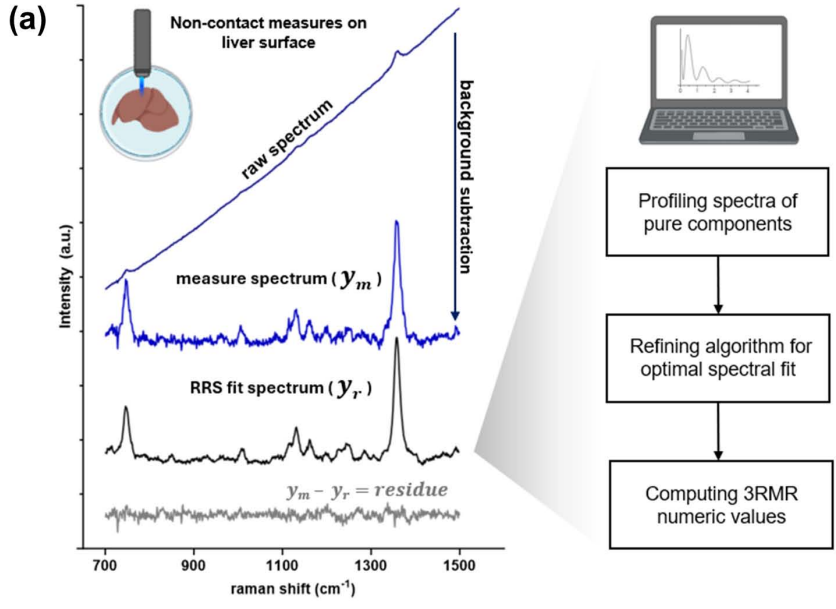
(a)
Non-contact measures on liver surface
raw spectrum
background subtraction
measure spectrum (y_m)
RRS fit spectrum (y_r)
$y_m - y_r = residue$
Intensity (a.u.)
700
900
1100
1300
1500
raman shift (cm^{-1})
Profiling spectra of pure components
Refining algorithm for optimal spectral fit
Computing 3RMR numeric values

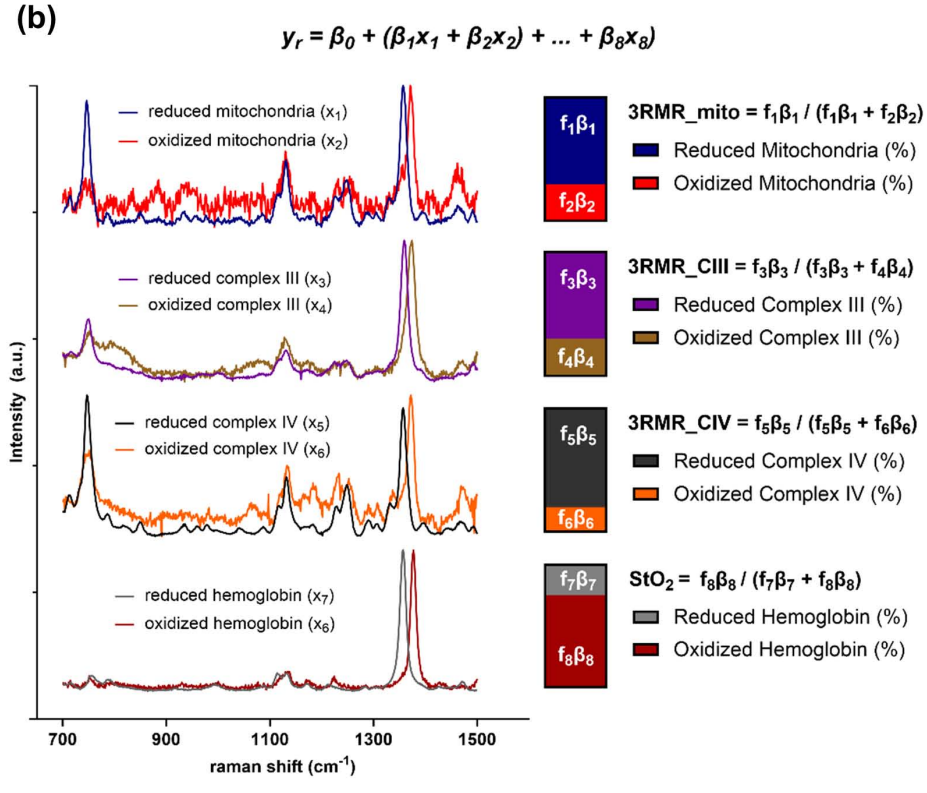
(b)
$y_r = \beta_0 + (\beta_1 x_1 + \beta_2 x_2) + \ldots + \beta_8 x_8)$
reduced mitochondria (x_1)
oxidized mitochondria (x_2)
reduced complex III (x_3)
oxidized complex III (x_4)
reduced complex IV (x_5)
oxidized complex IV (x_6)
reduced hemoglobin (x_7)
oxidized hemoglobin (x_6)
Intensity (a.u.)
700
900
1100
1300
1500
raman shift (cm^{-1})
$f_1\beta_1$
$f_2\beta_2$
3RMR_mito = $f_1\beta_1$ / ($f_1\beta_1$ + $f_2\beta_2$)
Reduced Mitochondria (%)
Oxidized Mitochondria (%)
$f_3\beta_3$
$f_4\beta_4$
3RMR_CIII = $f_3\beta_3$ / ($f_3\beta_3$ + $f_4\beta_4$)
Reduced Complex III (%)
Oxidized Complex III (%)
$f_5\beta_5$
$f_6\beta_6$
3RMR_CIV = $f_5\beta_5$ / ($f_5\beta_5$ + $f_6\beta_6$)
Reduced Complex IV (%)
Oxidized Complex IV (%)
$f_7\beta_7$
$f_8\beta_8$
StO_2 = $f_8\beta_8$ / ($f_7\beta_7$ + $f_8\beta_8$)
Reduced Hemoglobin (%)
Oxidized Hemoglobin (%)

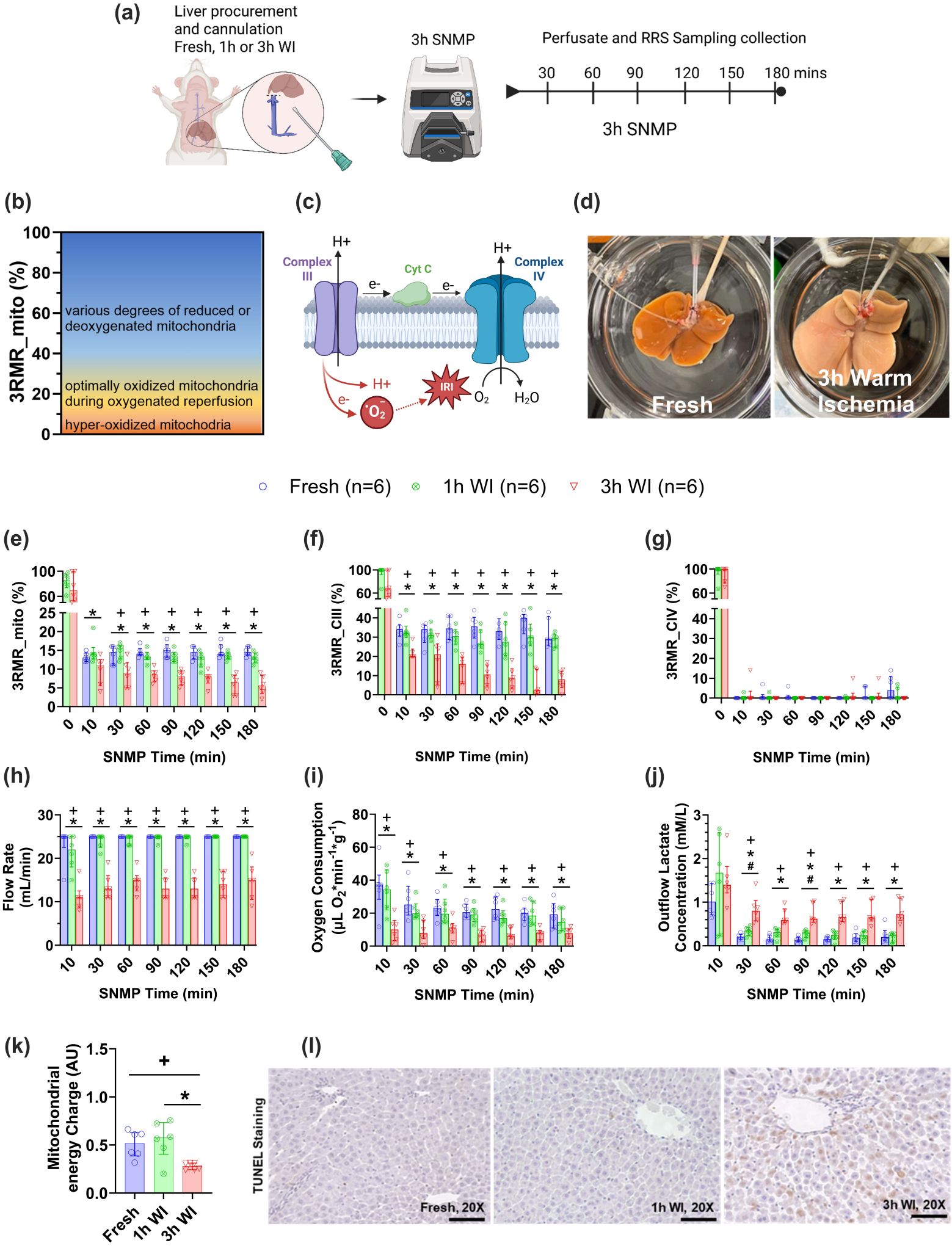
(a)
Liver procurement and cannulation Fresh, 1h or 3h WI
3h SNMP
Perfusate and RRS Sampling collection
30 60 90 120 150 180 mins
3h SNMP
(b)
3RMR_mito (%)
various degrees of reduced or deoxygenated mitochondria
optimally oxidized mitochondria during oxygenated reperfusion
hyper-oxidized mitochodria
(c)
Complex III
Cyt C
Complex IV
H+
e-
IRI
O2
H2O
(d)
Fresh
3h Warm Ischemia
Fresh (n=6)
1h WI (n=6)
3h WI (n=6)
(e)
3RMR_mito (%)
SNMP Time (min)
(f)
3RMR_CIII (%)
SNMP Time (min)
(g)
3RMR_CIV (%)
SNMP Time (min)
(h)
Flow Rate (mL/min)
SNMP Time (min)
(i)
Oxygen Consumption (µL O2*min-1*g-1)
SNMP Time (min)
(j)
Outflow Lactate Concentration (mM/L)
SNMP Time (min)
(k)
Mitochondrial energy Charge (AU)
Fresh
1h WI
3h WI
(l)
TUNEL Staining
Fresh, 20X
1h WI, 20X
3h WI, 20X


(a)
Fresh, 1h or 3h WI
Oxygen & Perfusate
Flow STOP
3RMR rapid rise
(~ 3mins)
Ongoing
SNMP
90 mins

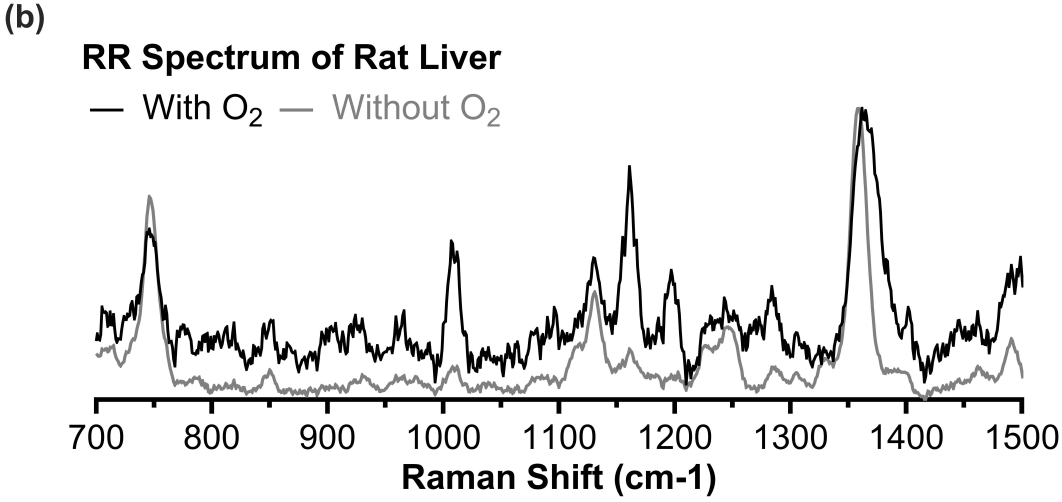
(b)
RR Spectrum of Rat Liver
With O2
Without O2
700
800
900
1000
1100
1200
1300
1400
1500
Raman Shift (cm-1)

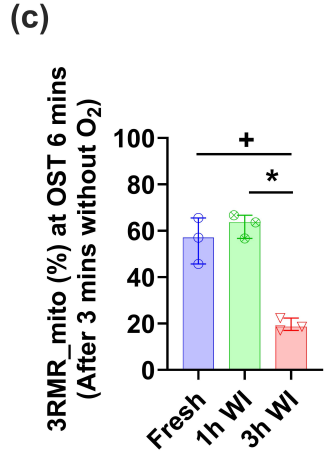
(c)
3RMR_mito (%) at OST 6 mins
(After 3 mins without O2)
100
80
60
40
20
0
+
*
Fresh
1h WI
3h WI

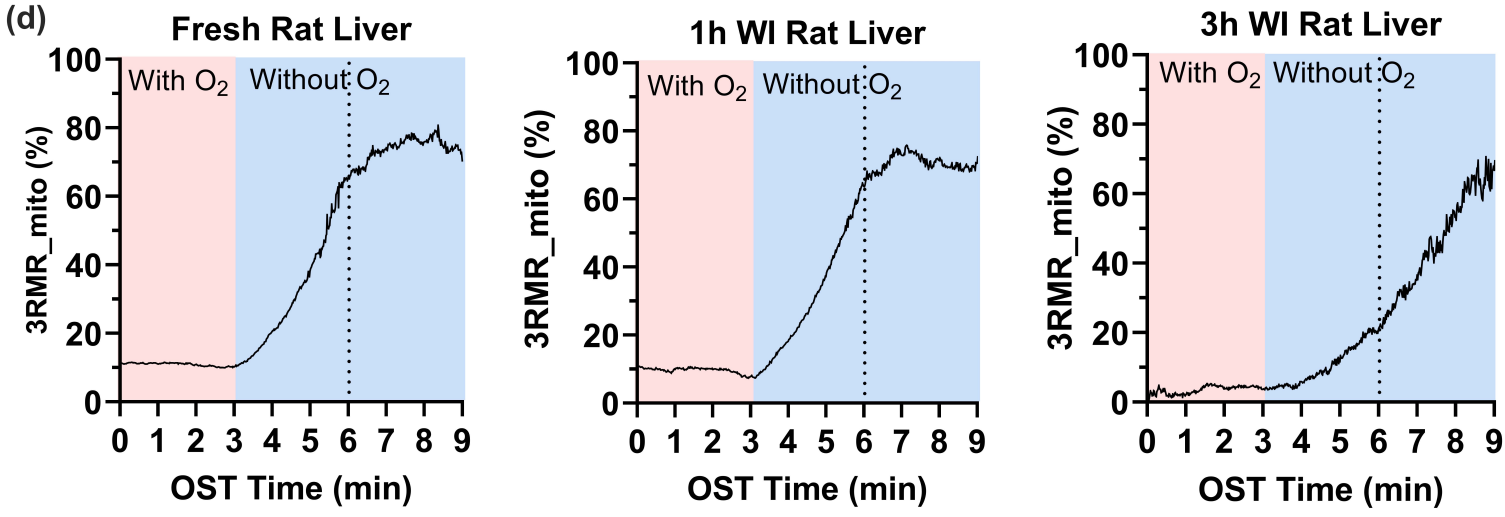
(d)
Fresh Rat Liver
1h WI Rat Liver
3h WI Rat Liver
With O2
Without O2
3RMR_mito (%)
OST Time (min)

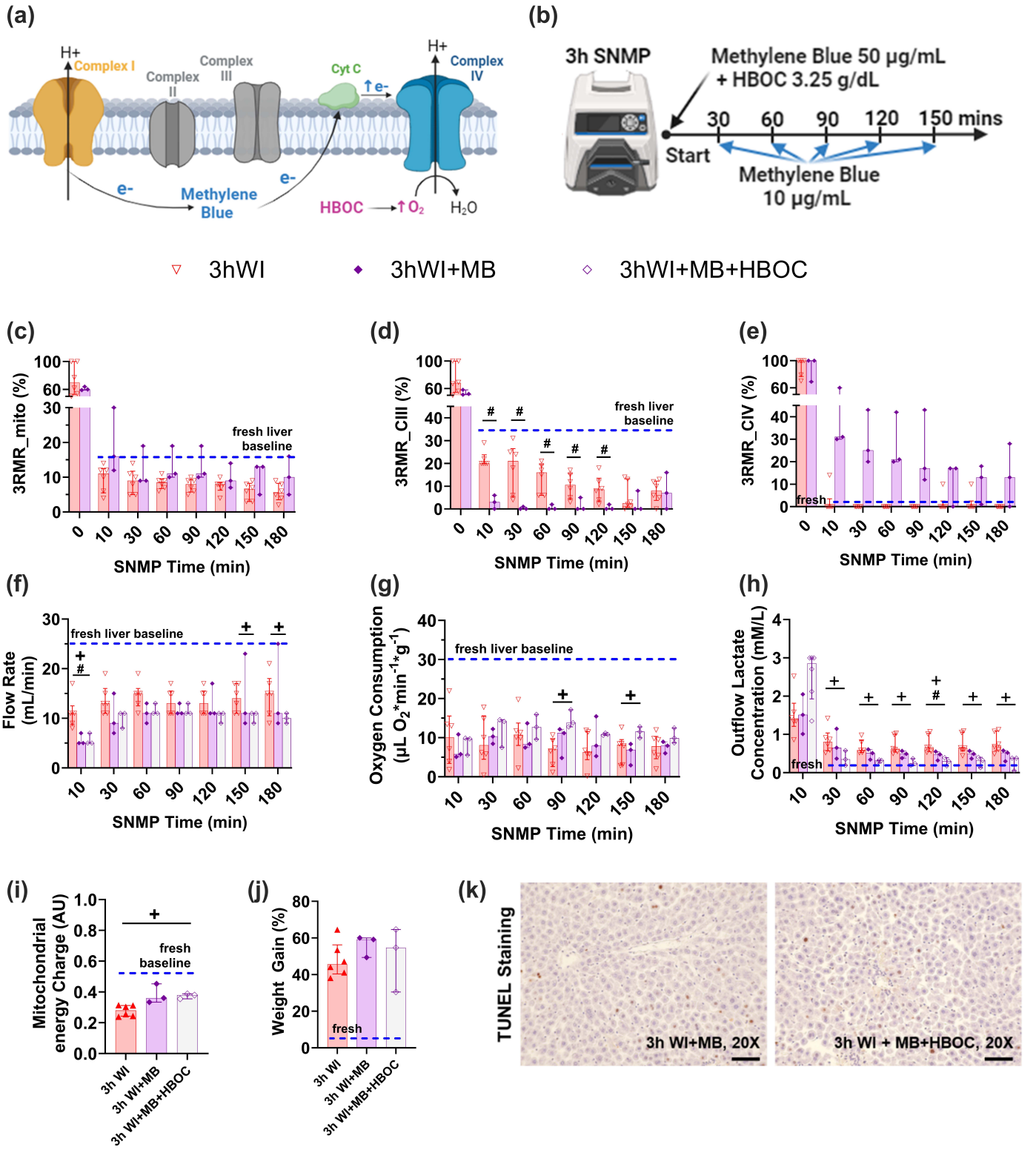
(a)
H+
Complex I
Complex II
Complex III
Cyt C
↑e-
H+
Complex IV
e-
Methylene Blue
e-
HBOC
↑O2
H2O
(b)
3h SNMP
Methylene Blue 50 µg/mL
+ HBOC 3.25 g/dL
30
60
90
120
150 mins
Start
Methylene Blue
10 µg/mL
3hWI
3hWI+MB
3hWI+MB+HBOC
(c)
3RMR_mito (%)
fresh liver baseline
SNMP Time (min)
(d)
3RMR_CIII (%)
fresh liver baseline
SNMP Time (min)
(e)
3RMR_CIV (%)
fresh
SNMP Time (min)
(f)
Flow Rate (mL/min)
fresh liver baseline
SNMP Time (min)
(g)
Oxygen Consumption (µL O2*min-1*g-1)
fresh liver baseline
SNMP Time (min)
(h)
Outflow Lactate Concentration (mM/L)
fresh
SNMP Time (min)
(i)
Mitochondrial energy Charge (AU)
fresh baseline
3h WI
3h WI+MB
3h WI+MB+HBOC
(j)
Weight Gain (%)
fresh
3h WI
3h WI+MB
3h WI+MB+HBOC
(k)
TUNEL Staining
3h WI+MB, 20X
3h WI + MB+HBOC, 20X

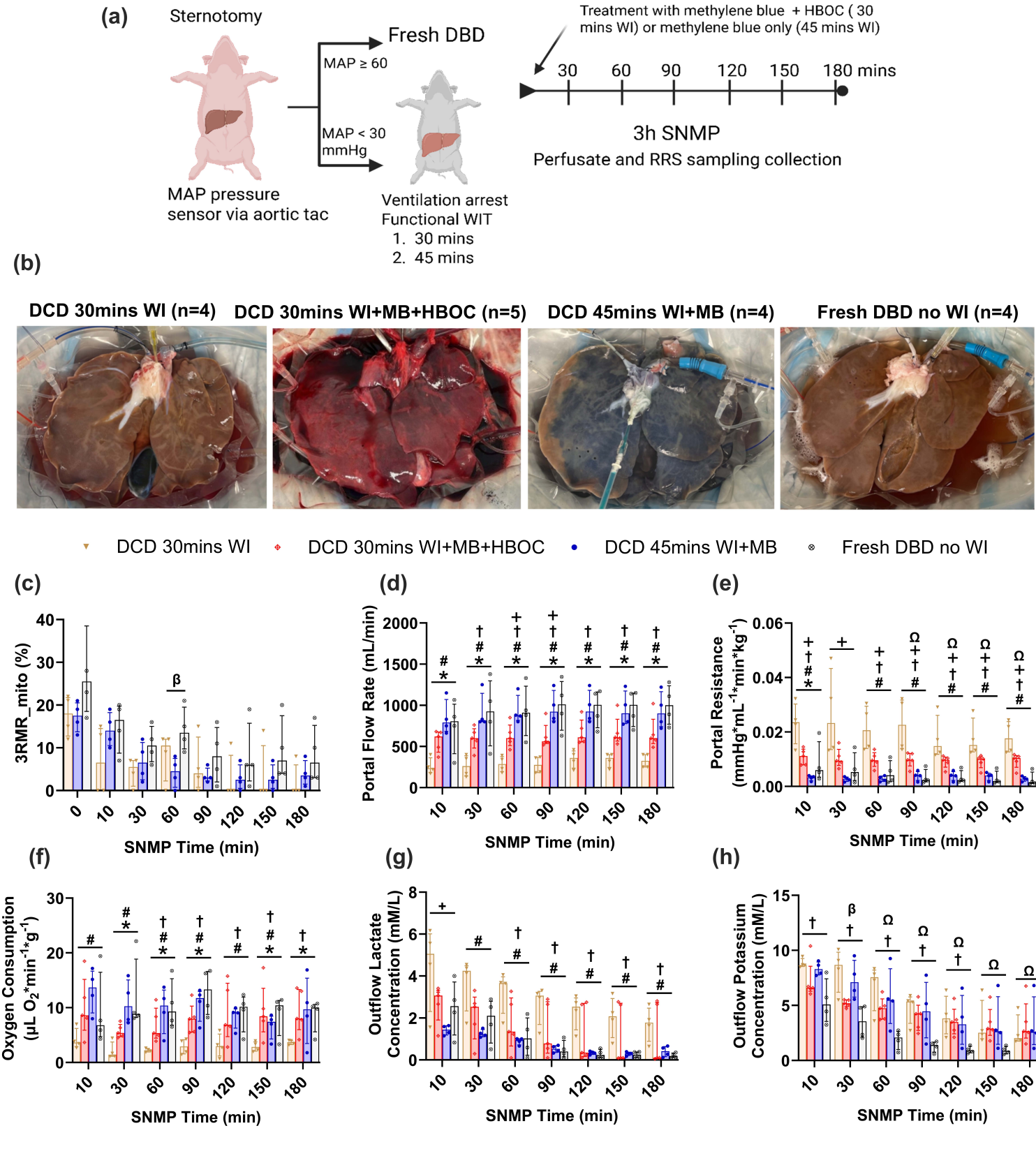
(a)
Sternotomy
Fresh DBD
MAP ≥ 60
MAP < 30 mmHg
MAP pressure sensor via aortic tac
Ventilation arrest
Functional WIT
1. 30 mins
2. 45 mins
Treatment with methylene blue + HBOC (30 mins WI) or methylene blue only (45 mins WI)
30 60 90 120 150 180 mins
3h SNMP
Perfusate and RRS sampling collection
(b)
DCD 30mins WI (n=4)
DCD 30mins WI+MB+HBOC (n=5)
DCD 45mins WI+MB (n=4)
Fresh DBD no WI (n=4)
DCD 30mins WI
DCD 30mins WI+MB+HBOC
DCD 45mins WI+MB
Fresh DBD no WI
(c)
3RMR_mito (%)
SNMP Time (min)
(d)
Portal Flow Rate (mL/min)
SNMP Time (min)
(e)
Portal Resistance (mmHg*mL-1*min*kg-1)
SNMP Time (min)
(f)
Oxygen Consumption (µL O2*min-1*g-1)
SNMP Time (min)
(g)
Outflow Lactate Concentration (mM/L)
SNMP Time (min)
(h)
Outflow Potassium Concentration (mM/L)
SNMP Time (min)